doi:10.1038/nature10330

Contents

Supplementary Discussion

Please note: in the supplement the residues are listed with subunit name in the prefix; residues conserved between all three antiporter-like subunits are indicated by an asterisk.

1. Description of proton-translocation pathways in antiporter-like subunits.

Possible pathways and intra-protein cavities were examined with programs CAVER[61], HOLE[62] and VOIDOO[63]. None of the channels is solvent-accessible on both sides of the membrane, with either 1.4 or 1.2 Å[62] radius probes.

In the first channel (near TM7), the cavity surrounding LysTM7 is about 70 Å^3, sufficient to hold up to two water molecules. One is observed in NuoN, near the C-terminus of TM7a. It is possible that less well-ordered water molecules are present in the similar positions in NuoL/M. In addition to LysTM7 and GluTM5, between 2 and 5 polar residues line this cavity (Fig. 4a-c and Supplementary Table 5). In all three subunits the channel is closed from the periplasm by a bulky residue just 'below' LysTM7 ($_L$Trp143, $_M$Trp143 and $_N$Ile132), followed by a tightly packed layer of hydrophobic residues. In NuoM, the path to the cytoplasm from LysTM7 is open for the 1.2 Å probe, reaching the surface near Glu108 and His159 *via* Asp258 (Fig. 4b). In NuoN, the protonation pathway from LysTM7 to the cytoplasm could include a putative water molecule between Tyr159 and Ser239, reaching the surface *via* conserved Lys295 and nearby Asp355/Asp357 (Fig. 4c). In NuoL, connection to a small cavity near His100 and further on to the cytoplasm can be achieved *via* a cavity next to Thr257. Additionally, a large cavity (about 200 Å^3) between NuoL and M is lined with polar residues. It is blocked from the periplasm by bulky hydrophobic residues, but is accessible to the cytoplasm *via* $_L$Arg115 or $_M$His441. Indeed, we observe a likely water molecule coordinated by invariant $_L$Arg175 and $_L$Glu144. Thus, protonation of LysTM7 in NuoL may be achieved also by “side-entry” near GluTM5 (Fig. 4a). Unlike NuoM and N, NuoL contains another invariant charged residue between GluTM5 and LysTM7, Asp178, needed for full activity[27]. A cavity (about 100 Å^3) between NuoM and N, near $_M$GluTM5 and $_N$LysTM12, is closed from the periplasm by hydrophobic residues. Access to the cytoplasm could be achieved if a water molecule is coordinated near $_M$Tyr151 and $_M$Thr172.

The cavity in the middle of the second channel, near Lys/GluTM12, is significantly larger and more polar than that in the first one. It is up to 200 Å^3 and is lined with about

ten polar residues (Fig. 4a-c and Supplementary Table 5). Two water molecules are observed in this cavity in NuoM and one in NuoN. Access to the cytoplasm from this cavity appears to be closed in all three subunits. However, the periplasm is accessible: in NuoL, Asp400 (conserved and important for proton pumping[27]) faces the cavity and can interact with Glu494, exposed at the likely lipid-periplasm interface. In NuoM, a path for the 1.2 Å probe is open *via* a small cavity lined with Ser414, Ser425 and Thr422, with only a short constriction near Thr332 at the surface. In NuoN, only Leu407 from the surface-exposed loop partly blocks the entrance to the channel, which is not likely to prevent access in the dynamic protein structure.

The connection between the two channels in each subunit is formed by many conserved charged and polar residues in the middle of the membrane (Fig. 4, Supplementary Fig. 8 and Table 5). The link between the channels is most obvious in NuoN: LysTM7 – W (observed water molecule) – Lys247 – W – His305 – W – LysTM12 (Fig. 4c). Although the distances between ionizable residues and resolved water molecules are 4-6 Å, there are no obstacles between them. Therefore, proton transfer is likely to be efficient, due to conformational flexibility and/or the presence of additional water molecules, probable due to the abundance of polar residues around this pathway. Some waters may be coordinated (also in NuoL/M) by the exposed backbone carbonyls from the π-bulge of TM8. Additionally, Tyr231 and Tyr333 nearby may participate in proton transfer, as suggested for a conserved tyrosine in cytochrome *c* oxidase[64]. Importantly, central $_{N}$Lys247 is invariant, essential for activity[28] and is found on the TM8 π-bulge. In NuoM, Lys265 is in a similar position between the two channels, and is also invariant and essential[30,31]. The pathway between the channels in NuoM thus is likely to involve His248, Lys265, His348 and invariant His322, as well as resolved and putative water molecules (Fig. 4b). In NuoL, an analog of $_{N}$Lys247 is absent, but in this area there is His254 and also Lys342, both invariant. Therefore, the pathway between the channels is likely to involve His254, Lys342, His338, His334 and putative water molecules (Fig. 4a).

Thus, in all antiporter-like subunits, two half-closed channels are linked in the middle of the membrane, forming a single continuous proton translocation pathway through each subunit. Similar to NuoL/M and NuoM/N cavities, the cavity at the NuoN/K/J interface might also be used for “side-entry” protonation of LysTM7 in NuoN *via* GluTM5. Thus, the additional input pathway to LysTM7 from the inter-subunit cavity

seems possible in all antiporter-like subunits. However, it is less likely compared to the first half-channel, since (in contrast to the NuoN/K/J interface) the NuoL/M and M/N interfaces are not extensive and so not well suited for active proton transport. The first half-channel also works better from the point of view of symmetry in conformational coupling, and residues lining it are more conserved than those at the interfaces. The overall architecture with two interacting anti-symmetrical half-channels may help achieve a high efficiency of coupling between the protein conformation and pmf, since nearly the entire subunit (rather than a single isolated channel of 3-4 helices) would be involved in proton translocation.

Overall, the periplasmic side of the protein is closed from the solvent more tightly, by bulky hydrophobic residues, probably because proton concentration here is higher compared to the cytoplasm. Large water-containing cavities in the second channel may serve to reduce the energy barrier for protons crossing the membrane, as observed in other proton pumps[65].

2. Are there alternative possibilities for the proton-translocation pathway in antiporter-like subunits?

What are the alternatives to the proposed pathway through two connected half-channels? A single fully functioning channel in only one of the two symmetry-related domains is unlikely, because the first channel, containing crucial LysTM7/GluTM5, is clearly functional and the second channel contains larger cavities with larger amount of conserved (some essential) polar residues, so must also be functional. A remote possibility is that GluTM5/LysTM7 act just as a conformational switch for the second channel. That is unlikely, since the first channel contains other polar residues and cavities linking it to the cytoplasm. Could both channels function as proton pumps? Then at least six protons would be translocated per cycle - such a stoichiometry is not thermodynamically feasible and has not been observed. Could one channel be used for proton transport and another for sodium (passive sodium antiport is suggested for complex I[66], but remains controversial)? This is unlikely since many conserved (some essential) polar residues form a connection between the two channels, which is needed only if both channels are half-closed.

We built homology models (not shown) for the antiporter subunits MrpA and MrpD (NuoL and NuoM homologues respectively), which also suggest two half-closed channels

connected by charged residues. Effects of mutations are consistent (Supplementary Table 8), suggesting that Mrp antiporters employ similar pathways and mechanisms for proton translocation. They couple, probably also conformationally, proton influx into the cell (*i.e.* in the same direction as during reverse reaction in complex I) to sodium efflux[26], with the sodium binding site possibly found in subunits MrpE-G or at the MrpA/D interface. Sequence conservation suggests that antiporter-like subunits in chloroplast Ndh complexes and membrane-bound hydrogenases are also likely to employ similar pathways.

3. Description of the proposed mechanism of coupling between electron transfer and proton translocation.

We observed that upon reduction of the hydrophilic domain by NADH helix $_{B}$H1 and the four-helix bundle from NuoD shift[13]. They are at the interface with the membrane domain and so can drive conformational changes there, in particular in subunits NuoA/J/K, through either direct contact (NuoD to NuoA) or *via* NuoH (Fig. 1c). Consistently, cross-links between NuoA and J disappear upon reduction of complex I[67]. Communication between the two domains may proceed in part *via* the long rigid helix TM1 of NuoH[11], which approaches close to TMs 1-3 of NuoJ with one end (Fig. 1c) and, with another end, close to helix $_{B}$H1 (which is linked to Fe-S cluster N2[13]). A short periplasmic helix of NuoJ, preceding $_{J}$TM5, may provide a connection between $_{H}$TM1 and the βH element (Fig. 3a).

Helix HL interacts with subunits NuoJ/K *via* $_{L}$TM16, so it can be moved, piston rod-like, along the membrane domain surface. HL in turn contacts flexible (due to an intra-helical loop) $_{LMN}$TM7, so it can change the environment of LysTM7, including the distance to GluTM5. Although lysine would be an unusual proton translocator due to its high pKa (~10), this value can be lowered by 3-4 pH units for a buried residue, as in the ApcT transporter[68]. Decrease in the distance between GluTM5 and LysTM7 will raise the pKa of lysine (due to approaching negative charge of carboxylate) and may result in its protonation (and *vice versa,* lysine deprotonation upon increase of distance).

Although helix HL is an obvious coupling element, it is likely to be not the only one. The βH element can interact with TM12 through the C-terminus of TM14 (linked to helix CH and hydrogen bonded to semi-conserved $_{L}$Trp67 / $_{M}$Trp71 from the hairpin).

TM14 can be mobile because it is short and highly tilted, resembling, together with helix CH, a broken TM helix (Fig. 3b). Additionally, interaction between the two half-channels from neighboring subunits is possible through an invariant proline in the TM12 intra-helical loop ($_{M}$Pro399* and $_{N}$Pro387*), which contacts GluTM5 from subunit NuoL and M, respectively. Conformational changes can push the proline against GluTM5, in turn changing its distance to LysTM7. The required flexibility of TM5 can be provided by another proline (conserved in NuoM, Pro149), which introduces a slight kink in the helix. Although this proline is absent in NuoL, $_{L}$TM5 contains three conserved glycines.

Interaction between the two half-channels in the same subunit can be mediated by TM8. Invariant $_{N}$Lys247, $_{M}$Lys265 and $_{L}$His254, connecting the two channels, are located on TM8 near its flexible kink. The βH element includes conserved (also in Mrp antiporters) salt bridges between the hairpin ($_{M}$Asp84*) and the C-terminus of TM8 ($_{M}$Arg273*, Fig. 3a). On the other hand, the N-terminus of TM8 is connected to TM7 by a very short rigid loop containing a conserved proline ($_{M}$Pro252*).

In NuoL, connecting helix CH is mostly unwound. However, $_{L}$TM8 is one of the most conserved TM helices in the complex, suggesting that its role in coupling may be relatively greater in NuoL than in NuoM/N.

The conformational changes, driven by the βH element and TM8, can result in protonation/deprotonation of Lys/GluTM12 *via* interactions with the exposed C-terminus of TM12a or with nearby charged residues - $_{N}$His305, invariant $_{M}$His322 and invariant $_{L}$His334. The exposure of GluTM5 and Lys/GluTM12 to the inter-subunit cavities suggests an additional possibility. These residues may switch between the two conformations. In one, as observed in the current structure and probably representing the oxidised enzyme, GluTM5 is closer to LysTM7 of the same subunit. Upon enzyme reduction, it could approach closer to Lys/GluTM12 on the nearby subunit, increasing its pKa and leading to its protonation by the incoming proton from the first channel of that subunit. In this way, protonation of the crucial residue in the opposite half-channels would be achieved in different parts of the catalytic cycle, as required for the directionality of the pump. The distance from $_{M}$Glu144 to $_{M}$Lys234 (5.4 Å) is only 2.8 Å shorter than the distance to $_{N}$Lys395, so such a mechanism appears plausible. It is not exclusively necessary, as LysTM12 in NuoL clearly operates without such a partner. In NuoN, GluTM5 also does not face another antiporter-like subunit, although it may interact with $_{K}$Glu72, at the beginning of the fourth proton pathway. Mutagenesis studies

support "switch" possibility – when GluTM5 in NuoM was shifted one helix turn up or down[69], the activity was retained (Supplementary Table 6, E144A/F140E and E144A/L147E mutants). Only in these positions the residue mutated to glutamate is not only close to LysTM7, but is also at the interface with NuoN. In other cases activity was lost even if the residue is close to LysTM7 (E144A/M146E).

Since the reaction of complex I is fully reversible (pmf can drive reduction of NAD^+ by ubiquinol), oxidoreductase activity must be tightly coupled to the conformational changes. A possible explanation for such coupling is the necessity for ubiquinone to be moved, by conformational changes, 10-20 Å out of the membrane[11] in order to react with its electron donor, cluster N2. Conversely, such quinone movement may assist conformational changes, through interaction of charged (semi)quinone species with charged residues in the vicinity (and/or cluster N2). Therefore, if mutations of residues in the proton channels interfere with conformational changes, oxidoreductase activity would be affected also, as observed (Supplementary Tables 6 and 7). Two of the most common mutations causing human diseases involve residues near $_M$TM7 and channel 4 (Supplementary Table 7).

Since the structure renders additional "direct" coupling unnecessary, it is unlikely that unusual disconnection of tandem coordinating cysteines from cluster N2 (observed upon reduction), will result in an additional translocated proton, as discussed previously[13]. However, such a change in N2 coordination helps to explain the reverse complex I reaction – pmf-driven conformational changes can shift helix H1 of NuoB, resulting in mechanical disconnection of the tandem cysteine(s), thus decreasing the redox potential of cluster N2 so that it can mediate reduction of NAD^+ *via* the chain of clusters. Conversely, in the forward reaction, disconnection of tandem cysteines upon N2 reduction will help drive conformational changes.

4. Are there any ubiquinone binding sites in the antiporter-like subunits, and is NuoN functionally different from NuoL/M?

In addition to the well-established ubiquinone-binding site at the interface of membrane and hydrophilic domains, quinone binding by antiporter-like subunits of complex I is also widely discussed in literature. On one hand, this is stimulated by photoaffinity labelling experiments with analogues of specific hydrophobic inhibitors, showing labelling of ND2[70], ND4[71] and ND5[36] subunits of bovine complex I,

homologous to *E. coli* NuoN, M and L, respectively. On the other hand, the presence of the quinone-binding motif (L/A-X_3-H-$X_{2/3}$-L/T/S) in these subunits has been proposed by Fischer and Rich[34]. In this motif, the conserved histidine residue serves as a hydrogen bond donor to quinone carbonyl or hydroxyl moieties, while the quinone ring is usually flanked by aromatic and aliphatic residues.

The signature motif is quite weak and authors suggested that it can be more indicative of the true quinone-binding site when combined with high sequence conservation in the same region. Sequence motifs centred on $_{L}$His334, $_{L}$His338, $_{M}$His241, $_{M}$His322, $_{M}$His348 and $_{N}$His224 have been discussed as potential quinone binding sites[27,28,34]. In addition, Amarneh and Vik[28] observed inhibition of NADH oxidase activity by decylubiquinone in several mutants, including $_{N}$His224. The structure shows that the majority of these histidines are in fact buried deep inside the protein and are parts of putative proton translocation channels. Only $_{M}$His241 and $_{N}$His224 (structurally and sequentially conserved) are located on TM7b pointing outside the subunit. However, they interact directly with helix HL, which is the likely primary reason for their conservation. Importantly, inhibition (or lack of activation) with decylubiquinone were also observed for mutations[28] of other surface residues interacting with HL, $_{N}$Lys158 and $_{N}$Tyr300. Recently, analogous residues in NuoL and NuoM ($_{L}$Lys169, $_{M}$Lys173, $_{L}$Gln236 and $_{M}$His241), all contacting HL (Fig. 3a and Supplementary Table 6), were mutated, with similar results for all three antiporter-like subunits[38]. Thus, the effect of these mutations cannot be attributed to disruption of any additional quinone binding sites. Rather, it occurs due to interference with conformational coupling, likely involving communication between helix HL and the quinone-binding site at the interface with the hydrophilic domain. Both proton-pumping and oxidoreductase activities were significantly affected in these mutants[38], confirming essential coupling role of helix HL.

Thus, we do not see any potential quinone binding sites in antiporter-like subunits, either formed around these histidines or elsewhere. The labelling by photoaffinity inhibitor analogues may have been unspecific, for example due to the presence of hydrophobic crevices at the interfaces between subunits. Global conformational changes upon enzyme reduction or inhibitor binding would explain the effects observed on labelling[36].

Also, one tightly bound quinone molecule[72], as well as two semiquinone species, have been observed in bovine complex I[4]. Fast-relaxing semiquinone (Q_{Nf}) is sensitive to the membrane potential and interacts with cluster N2, whilst slow-relaxing semiquinone

(Q_{Ns}) is not[4,35]. Additionally, mutations to GluTM5 in NuoN appear to affect activity less drastically than in NuoL/M[28], and it was noted earlier[15] and discussed in detail recently[73] that TMs 1-3 are absent from NuoN in metazoans. These observations led to the proposals that subunit NuoN is functionally different from NuoL/M, does not pump protons and contains bound quinone acting as a cofactor (Q_{Ns})[35,44,73].

The structure indicates that this is unlikely, since TMs 1-3 are found at the periphery of antiporter-like subunits and only helices 4-13 form the functional core, which is very similar in NuoL, M and N. Also, the β-hairpin between TMs 2 and 3 is short in NuoN and its role in metazoans may be performed by supernumerary subunit(s). Additionally, TM1 is absent in NuoL from insects (*D. melanogaster*) and worms (*C. elegans*) (Supplementary Fig. 8).

Furthermore, although the NuoN environment is fully preserved in the structure (all subunits contacting it are present), we do not observe any bound cofactors. A likely explanation for the presence of two observed semiquinone species is that one of them (Q_{Ns}) represents the population of quinone molecules bound as in the oxidised state of complex I, fully embedded in the membrane and thus far away from cluster N2. The other species (Q_{Nf}) may represent quinone moved out of the membrane[11] by conformational changes, so that it can interact with cluster N2.

The difference in effects of GluTM5 mutations can be explained if inter-subunit interactions *via* GluTM5 are important to sustain conformational changes in antiporter-like subunits, as we describe for NuoL and M. However, in NuoN the equivalent $_{N}$Glu133 does not face another antiporter-like subunit. Consequently, mutations may not impede overall conformational change and hence activity. Although proton pumping by NuoN is likely to be compromised by mutations, a drop in overall stoichiometry from 4 to 3 is difficult to measure experimentally. It was also noted that $_{N}$Glu133 is not conserved in worms[38,73]. However, these species show other sequence deviations and lack also $_{K}$Glu72 / $_{J}$Tyr59 (Supplementary Fig. 8), so it is possible that channel 4, involving all three residues, is not functional in worms. On the other hand, all three crucial lysines (217, 247 and 395) are conserved in NuoN from these species, so this subunit is still likely involved in proton pumping, with the modulating role of $_{N}$Glu133 taken over by other residue(s). Mutations of any of these lysines in NuoN completely abolish activity in *E. coli*[28], supporting the notion that NuoN pumps protons similarly to NuoL/M.

In a recent publication[37] it was shown that when helix HL is truncated (or subunit NuoL removed completely), oxidoreductase activity remains, but proton-pumping is

diminished, confirming the essential coupling role of this helix. The proton-pumping assays were very qualitative, and any known quantitative measures[42,74] were not employed. Therefore, even though it was suggested that proton-pumping stoichiometry dropped from 4 to 2, this value is hardly reliable. Importantly, however, even if this estimation turns out to be correct, it does not mean that the 2 remaining protons are pumped *via* direct redox coupling involving two quinones and that NuoN does not pump protons, as the authors suggest[37]. Our structure shows that discontinuous helix TM7 in subunit NuoN contacts helix HL at its extremity, were HL is continued by $_{L}$TM16, at the interface with subunits NuoAJK (Fig. 1ab). As we propose, conformational changes in NuoAJK drive $_{L}$TM16 and HL, which then communicates with distal subunits NuoM/L. Truncation of HL will abolish this communication and so the translocation of two protons *via* NuoM/L. However, since TM7 in NuoN is in close contact with NuoAJK, NuoN can still perform proton translocation within our mechanism. The fourth proton channel is found at NuoN/K/J interface and so clearly may perform translocation without HL. So, in full agreement with our model, HL-truncated mutants can still translocate two protons per cycle.

In another recent proposal it is suggested that complex I contains only two functioning proton pump modules, one in each of the two halves of the membrane domain (divided as NuoHAJKN and NuoLM sub-complexes)[75]. During the catalytic cycle each pump would perform two “strokes”, resulting in four protons translocated in total. This model implies that either NuoM or NuoL subunit is not functional, which appears highly unlikely in view of the many conserved and essential (Supplementary Table 6) charged residues found in the proton translocation channels in both subunits.

In summary, the structure does not provide support for the presence of any additional quinone-binding sites in antiporter-like subunits, nor for proposals that subunit NuoN is functionally different from NuoL/M. The presence of a single Q-site at the interface of the two main domains, involving subunit NuoH (Fig. 1c), is consistent with all available functional and mutagenesis data.

Supplementary Table 1. Data collection, phasing and refinement statistics.

	Native		SeMet	
Data collection				
Beamline	ID29		ID29	
Space group	P1		P1	
Cell dimensions				
a, *b*, *c* (Å)	95.59, 116.79, 191.84		93.67, 116.23, 189.28	
α, β, γ (º)	98.40, 104.23, 108.60		98.31, 102.66, 109.24	
		Peak	*Inflection*	*Remote*
Wavelength (Å)	1.00	0.9789	0.9790	0.85
Scaling 1				
Resolution (Å)	30-3.2 (3.37-3.20)	30-3.5 (3.69-3.50)	30-3.60 (3.79-3.60)	30-3.7 (3.90-3.70)
R_{sym} or R_{merge} (%)	13.8 (73.2)	21.2 (101.9)	18.5 (88.2)	24.6 (100.1)
R_{pim} (%)	10.0 (55.2)	12.6 (60.4)	11.0 (52.3)	13.4 (54.7)
$I/\sigma I$	4.9 (1.3)	4.7 (1.3)	5.7 (1.5)	4.7 (1.5)
Completeness (%)	95.4 (96.1)	97.3 (97.7)	97.4 (97.7)	97.8 (98.0)
Redundancy	2.5	3.8	3.8	4.4
Scaling 2 (anisotropically truncated data)				
Resolution (Å)	30-3.0 (3.16-3.0)			
R_{sym} or R_{merge} (%)	16.4 (121.6)			
R_{pim} (%)	12.0 (92.0)			
$I/\sigma I$	4.1 (0.8)			
Completeness (%)	95.5 (96.0)			
Redundancy	2.6 (2.6)			
Completeness after aniso truncation (%)	86.5 (54.0)			
Refinement				
Resolution (Å)	20-3.0			
No. reflections	126323			
R_{work}/ R_{free} (%)	23.19/28.16			
No. atoms	30310			
Protein	30002			
Ligand/ion	292			
Water	16			
Mean B-factors (Å^{-2})	76			
R.m.s deviations				
Bond lengths (Å)	0.016			
Bond angles (º)	1.070			

*Highest resolution shell is shown in parenthesis.
Scaling 1 and refinement to 3.2 Å were performed using all data as a control, yielding R_{work}/R_{free}=23.1/27.4 %. The main refinement was performed with data anisotropically scaled and truncated to 3.4, 3.0 and 3.0 Å along *a**, *b** and *c** axes respectively (Scaling 2).

Supplementary Table 2. Residues present in the model.

Subunit	Number of residues in sequence	Residues built	Missing fragments
NuoL	613	1-612	C-terminus
NuoM	509	1-504	C-terminus
NuoN	485	1-191, 199-439, 445-485	Fragments of TM6 -TM7 loop and TM13 -TM14 loop
NuoK	100	1-100	None
NuoA	147	15-43, 61-126	Loop TM1-TM2, C and N termini
NuoJ	184	1-168	C-terminus

Supplementary Table 3. Statistics of structural alignment of subunits NuoL, M and N, their symmetry related domains and subunit NuoK.

a) Antiporter-like subunits, 14 conserved TM helices.

Subunits	RMSD Cα, Å	Length of alignment	Sequence Identity, %
NuoL-NuoM	1.73	437	22.0
NuoL-NuoN	2.15	421	20.2
NuoM-NuoN	2.16	418	19.4

b) Symmetrical sets of five helices.
The letter signifies subunit, the number - set of helices:
1 - TM 4-8, 2 – TM 9-13.

Set of helices	RMSD Cα, Å	Length of alignment	Sequence Identity, %
L1-L2	2.22	136	10.3
M1-M2	3.09	137	9.5
N1-N2	2.91	148	12.2

c) Alignment of subunit NuoK with TM helices 4-6 (set 1) and 9-11 (set 2) of antiporter-like subunits. Naming convention as in table **b**.

Alignment	RMSD Cα, Å	Length of alignment	Sequence Identity, %
K-L1	2.66	85	18.7
K-L2	2.13	79	11.4
K-M1	2.20	78	10.3
K-M2	3.48	86	9.2
K-N1	1.95	88	17.0
K-N2	2.19	89	10.1

Supplementary Table 4. Summary of analysis of interactions between subunits.

a) Membrane domain assembly (subunits NuoLMNAJK)

Surface area, Å^2	62193.0	ΔG^{int}, kcal/mol	-322.3
Buried area, Å^2	30535.0	ΔG^{diss}, kcal/mol	76.6

b) Individual subunits

Range	**Surface area, Å^2**	**Buried area, Å^2**	**ΔG^{int} kcal/mol**	**N_{HB}**	**N_{SB}**
L	27186.8	4439.1	-44.63	19	3
M	18180.5	3981.5	-44.32	16	4
N	17841.3	6263.4	-66.26	24	7
K	7588.8	5846.4	-51.42	36	8
J	13595.9	7167.6	-85.47	25	6
A	8334.8	2837.0	-30.22	16	2

c) Pair-wise subunit interactions

Interfacing structures	**Buried area, Å^2**	**ΔG^{int}, kcal/mol**	**N_{HB}**	**N_{SB}**
A+J+K+N				
J + K	3347.2 (11%)	-63.9 (20%)	15 (22%)	3 (20%)
J + A	2171.4 (7%)	-51.9 (16%)	8 (12%)	2 (13%)
A + K	303.8 (1%)	-6.0 (2%)	5 (7%)	0 (0%)
K + N	1724.8 (6%)	-32.0 (10%)	12 (18%)	3 (20%)
A + N	361.7 (1%)	-7.5 (2%)	3 (4%)	0 (0%)
J + N	1317.6 (4%)	-30.8 (10%)	2 (3%)	1 (7%)
K + L	470.6 (2%)	-6.3 (2%)	4 (6%)	2 (13%)
J + L	331.4 (1%)	-8.8 (3%)	0 (0%)	0 (0%)
L+M+N				
M + L	2379.7 (8%)	-45.4 (14%)	12 (18%)[5]	1 (7%) [1]
N + M	1601.8 (5%)	-39.5 (12%)	4 (6%)	3 (20%)
N + L	1257.4 (4%)	-30.4 (9%)	3 (4%)	0 (0%)

Analysis was performed using the PISA server at PDBe (http://www.ebi.ac.uk/msd-srv/prot_int/cgi-bin/piserver). ΔG^{int} indicates the solvation free energy gain upon formation of the assembly, ΔG^{diss} indicates the free energy of assembly dissociation, N_{hb} – number of hydrogen bonds at the interface and N_{sb} – number of salt bridges at the interface. Numbers in square brackets indicate how many bonds between NuoM and NuoL are contributed by helix HL. All other subunits can contact NuoL only *via* HL and TM16.

Supplementary Table 4, continuation. Details of interactions between antiporter-like subunits. Contacts involving the β-hairpin are in blue, helix HL - in red. Potential weak hydrogen bonds are not included.

M+L

NuoM	Dist, Å	NuoL
Hydrogen bonds		
GLN 483[NE2]	2.75	SER 69[OG]
GLY 479[O]	2.88	TRP 67[NE1]
GLN 483[OE1]	2.99	SER 69[OG]
SER 379[OG]	3.45	TYR 158[OH]
GLN 416[NE2]	2.99	ASN 190[OD1]
SER 433[OG]	3.15	ARG 175[NE]
GLN 416[OE1]	3.63	TYR 189[OH]
TRP 303[NE1]	3.65	PHE 553[O]
TYR 317[OH]	2.51	ASP 563[OD1]
HIS 241[NE2]	2.63	ASP 563[OD2]
LYS 173[NZ]	2.79	ASN 566[OD1]
TYR 300[OH]	3.30	LEU 565[N]
Salt bridges		
HIS 241[NE2]	2.63	ASP 563[OD2]

N+M

NuoN	Dist, Å	NuoM
Hydrogen bonds		
VAL 469[O]	3.19	TRP 71[NE1]
GLN 472[OE1]	3.14	ARG 74[N]
GLU 324[OE2]	3.56	ARG 74[NE]
GLU 324[OE1]	3.69	ARG 74[NH2]
Salt bridges		
GLU 324[OE2]	3.56	ARG 74[NE]
GLU 324[OE1]	3.96	ARG 74[NE]
GLU 324[OE1]	3.69	ARG 74[NH2]

N+L

NuoN	Dist, Å	NuoL
Hydrogen bonds		
LYS 158[NZ]	3.60	TYR 594[OH]
ASP 229[OD2]	2.52	TYR 594[OH]
PRO 222[O]	3.31	SER 597[OG]

Supplementary Table 5. Residues forming putative proton translocation channels, either directly or by coordinating water molecules. Essential residues are in bold. In channel 4 prefix indicates subunit.

Sub-unit	Channel		Residues
NuoL	1	Main cavity	**K229**, D178, T174, S150, **E144**
		Main link to cytoplasm	T257, T120, H100
		Possible link at subunits' interface	R175, Y151, Y119, R115
	Connection		H254, K342, H338, T312, carbonyl O of A255
	2	Main cavity	**K399**, S398, T318, S314, Q315, T425, T428, S311, H334, T337, T429
		Link to periplasm	D400, S497, E494
NuoM	1	Main cavity	**K234**, T178, T266, **E144**
		Main link to cytoplasm	D258, S105, H117, E108, H159
		Possible link at subunits' interface	Q179, Y151, T172
	Connection		**K265**, H248, H348, S319, carbonyl O of A260 and G261
	2	Main cavity	**E407**, Q344, N403, S351, S321, H322, T395, T318, Y435, S436
		Link to periplasm	S414, S425, T422, T332
NuoN	1	Main cavity	**K217**, S136, S163, S167, S246, Y159, **E133**
		Main link to cytoplasm	S239, K295, D355, D357
		Possible link at subunits' interface	$_{K}$E72, T160, S156
	Connection		**K247**, S219, T227, Y231, S302, Y333, S337
	2	Main cavity	**K395**, Y308, Y329, H305, S418, S382, S336, S304, N285, S301, Y425, Y424
		Link to periplasm	S322
NuoN K/J/A	4	Main channel	$_{N}$S156, $_{N}$T160, $_{K}$**E72**, $_{K}$**E36**, $_{J}$**Y59**, $_{K}$N40, $_{J}$S35, $_{J}$E55, $_{K}$Y62, $_{K}$Q59, $_{K}$S51
		Alternative link to periplasm	$_{K}$S67, $_{A}$Y84, $_{A}$E81, $_{J}$S145, $_{J}$E142, $_{A}$E102

Supplementary Table 6. Mutations in the membrane domain of *E.coli* complex I. Residues conserved between all antiporter-like subunits are in bold, those conserved within a single subunit in regular font and those not conserved in italic. Oxidoreductase activities were measured with either O_2 or DQ as final acceptor and the range observed is shown. Proton pumping rates are very approximate. Abbreviations: SB - salt bridge, HB – hydrogen bond, HL – helix HL.

a) Mutations in subunit **NuoL**

Mutation	Amino acid location	Effect			Reference
		Expression	Activity	Proton pumping	
D82A	β-hairpin - TM8 SB	normal	90%	80%	27
D82N		normal	75%	80%	27
D134N	surface, interacts with β-hairpin	normal	110%	70%	27
E144A	channel 1/ interface with NuoM	reduced	20%	30%	27
E144Q		normal	15%	10%	27
K169C	TM6 – HL SB	normal	65%	decreased	38
K169E		normal	67%	decreased	38
K169R		normal	94%	decreased	38
D178A	channel 1	normal	95%	80%	27
D178N		normal	70%	50%	27
K229A	channel 1	low	10%	NA	27
K229R		normal	30%	NA	27
K229E		low	20%	NA	27
Q236H	TM7b – HL HB	normal	86%	NA	38
Q236K		normal	57%; DQ inhibition	significantly decreased	38
Q236C		normal	86%	NA	38
Q236E		normal	84%	NA	38
W238A	TM7b - TM7a HB	normal	80%	NA	27
W238Y		low	50%	NA	27
W238C		low	30%	NA	27
D303A	surface, interacts with TM11-12 loop	normal	110%	80%	27
D303N		normal	100%	80%	27
H334A	connecting	low	50%	NA	27
H334Q		normal	120%	NA	27
H338A		normal	100%	NA	27
H338Q		normal	100%	NA	27
E359A	surface	normal	100%	normal	27
K399A	channel 2	low	20%	NA	27
K399E		low	15%	NA	27

Supplementary Table 6, continuation.

a) Mutations in subunit **NuoL,** continuation.

Mutation	Amino acid location	Effect			Reference
		Expression	Activity	Proton pumping	
D400A	channel 2 / surface	normal	70%	50%	27
D400N		normal	90%	70%	27
D400E		normal	100%	90%	27
R431A	surface, near HL	low	10%	NA	27
R431H		normal	100%	NA	27

b) Mutations in subunit **NuoM**

Mutation	Amino acid location	Effect			Reference
		Expression	Activity	Proton pumping	
D84A	β-hairpin - TM8 SB	normal	83%	NA	76
D84N		normal	89%	NA	76
D135A	surface, interacts with β-hairpin	reduced	44%	normal	76
D135N		normal	78%	normal	76
D135E		normal	87%	normal	76
E144A	channel 1 / interface with NuoN	normal	2-10%	no pumping	76, 30, 69
E144Q		normal	2%	no pumping	76
E144D		normal	89-100%	normal	76, 30
E144A/M145E	channel 1 / interface with NuoN	normal	3%	no pumping	69
E144A/W143E		normal	13%	~15%	69
E144A/V148E		normal	3%	no pumping	69
E144A/F140E		normal	60%	~60%	69
E144A/F152E		normal	3%	no pumping	69
E144A/F141E		normal	3%	no pumping	69
E144A/L147E		normal	45%	~50%	69
E144A/F139E		normal	2%	no pumping	69
E144A/F142E		normal	3%	no pumping	69
E144A/M146E		normal	2%	no pumping	69
E144A/P149E		normal	4%	no pumping	69
E144A/M150E		normal	2%	no pumping	69
E144A/Y151E		normal	3%	no pumping	69
E144A/L153E		normal	3%	no pumping	69
E144A/V127E		normal	3%	no pumping	69
E144A/I128E		normal	3%	no pumping	69
E144A/G129E		normal	5%	no pumping	69
E144A/I189E		normal	3%	no pumping	69
E144A/L190E		normal	2%	no pumping	69
E144A/A191E		normal	3%	no pumping	69

Supplementary Table 6, continuation.

b) Mutations in subunit **NuoM,** continuation

Mutation	Amino acid location	Effect			Reference
		Expression	Activity	Proton pumping	
K173C	TM6 – HL HB	normal	70%	decreased	38
K173E		normal	50%	decreased	38
K173R		normal	91%	decreased	38
H196A	surface	normal	79%	NA	76
K234A	channel 1	normal	5-10%	significantly decreased	76, 30
K234R		slightly reduced	5-20%	significantly decreased	30
H241A	TM7b - HL interaction	normal	88%	NA	76
H241E		normal	71%	NA	38
H241K		normal	40%; DQ inhibition	significantly decreased	38
H241R		normal	46%	NA	38
W243A	TM7b – TM7a HB	Normal/ decreased	103%	normal	76, 30
W243Y		normal	104%	NA	76
P245A	TM7b surface	normal	102%	NA	76
K265A	connecting	normal	35-80%	normal to significantly decreased	76, 30
R273A	TM8 - β-hairpin SB	normal	92%	NA	76
H322A	channel 2	normal	100%	NA	76
H348A	connecting	normal	92%	NA	76
R365A	surface, SB TM11-TM14	normal	87%	*NA*	76
R369H	surface, HB to TM7b	normal	63%	normal	76
Y435A	channel 2	normal	99%	NA	76

Supplementary Table 6, continuation.

c) Mutations in subunit **NuoN**

Mutation	Amino acid location	Effect			Reference
		Expression	Activity	Proton pumping	
M1H	N-terminus, surface	normal	20%	100%	28
M74K	surface	normal	90%	100%	28
C88S	TM3, interior	normal	100%	100%	28
C88V		normal	100%	100%	28
E104C	surface, near NuoJ	normal	90%	100%	28
E133A	channel 1 / interface with NuoK	normal	70%	100%	28
E133C		normal	70%	100%	28
E133D		normal	80%	100%	28
R151C	surface	normal	90%	100%	28
E154C	surface, interacts with NuoK N-terminus	normal	70%	90%	28
K158C	TM6 – HL HB	normal	50%; DQ inhibition	80%	28, 38
K158R		normal	70%	80%	28, 38
K158E		normal	47%	reduced	38
T160I	interface with NuoK	normal	80%	NA	28
K217C	channel 1	No expression	NA	NA	28
K217R		normal	40%	80%	28
H224A	TM7b - HL interaction	normal	100%	100%	28
H224Y		normal	90%	100%	28
H224K		normal	40%; DQ inhibition	70%	28
H224E	TM7b - HL interaction	normal	67%	NA	38
H224R		normal	32%	NA	38
W226C	TM7b – TM7a HB	normal	90%	100%	28
D229C	TM7b – $_{L}$TM16 and HL interaction	normal	70%	100%	28
K247C	connecting	normal	0-7%	50%	28
K247R		normal	80%	100%	28
K295C	channel 1 ?	normal	80%	70%	28
K295R		normal	90%	80%	28
Y300C	TM10 - HL interaction	normal	70%; DQ±	80%	28
Y300S		normal	50%; DQ±	80%	28
G391S	near channel 2	normal	90%	NA	28
K395C	channel 2	normal	5%	NA	28
K395R		normal	30%	NA	28
Y424C	channel 2	normal	90%	NA	28
M482C	surface	normal	100%	NA	28

Supplementary Table 6, continuation.

d) Mutations in subunit **NuoK**

Mutation	Amino acid location	Effect			Reference
		Expression	Activity	Proton pumping	
F15A	interface with NuoN	normal	90%	NA	32
G21V	interface with NuoJ	normal	61%	NA	32
R25A	HBs to backbone of	normal	26%	~30%	32
R25K	$_{J}$TM1 C-terminus	normal	28-31%	NA	32
R26A	surface, near $_{L}$TM16	normal	39%	~40%	32
R26K		normal	100%	NA	32
R25A/R26A		normal	14%	~30%	32
E36A	channel 4, interface with NuoJ	normal	1-7%	NA	32
E36Q		normal	3-8%	no pumping	33, 32
E36D		normal	120%	normal	33
I39D	interface with NuoN	normal	140%	normal	33
A69D	opposite E36	normal	119%	normal	33
E36Q/E72Q		normal	5%	impaired	33
E36Q/I39D		normal	21%	impaired	33
E36Q/A69D		normal	91%	normal	33
E72A	channel 4, interface with NuoN	normal	43-48%	~50%	32
E72Q		normal	22-77%	~20%	33, 32
E72D		normal	100%	normal	33
E72Q/I39D		normal	180%	normal	33
E72Q/A69D		normal	77%	impaired	33
E72Q/G34D		normal	77%	impaired	33
E36Q/I39D/ A69D/E72Q		normal	200%	impaired	33
R85A	surface	normal	100%	NA	32
R85K		normal	98%	NA	32
R87A	surface	normal	99%	NA	32
R87K		normal	100%	NA	32

Supplementary Table 6, continuation.

e) Mutations in subunit **NuoA**

Mutation	Amino acid location	Effect			Reference
		Expression	Activity	Proton pumping	
K46A	TM1-TM2 loop, not in the structure	normal	94-100%	NA	77
E51A	TM1-TM2 loop, not in the structure	normal	30%	NA	77
D79A	interface between ȷTM3 and NuoH	normal	86-95%	NA	77
D79N		normal	37-44%	NA	77
E81A	alternative channel 4, interface with NuoJ	normal	~40%	NA	77
E81Q		normal	50-77%	NA	77
D79N/E81Q		normal	2-10%	NA	77

f) Mutations in subunit **NuoJ**

Mutation	Amino acid location	Effect			Reference
		Expression	Activity	Proton pumping	
Y59C	channel 4, interface with NuoK	normal	57-93%	normal	40, 41
Y59F		normal	44-50%	normal	40, 41
G61V	TM3 kink, interface with NuoA	normal	48-53%	normal	40
G61L		normal	69-72%	normal	40
M64V	near channel 4	normal	78-89%	~60%	40, 41
M64C		normal	47%	NA	41
M64I		normal	100%	normal	40, 41
V65G	near TM3 kink, interface with NuoA	normal	3-13%	No pumping	40, 41
V65L		normal	21-23%	reduced	40
F67A	near channel 4	normal	~85%	100%	40
M72V	interface with NuoA/H	NA	38%	NA	41
M72A		NA	74%	NA	41
M72C		NA	50%	NA	41
M64V/M72A		NA	92%	NA	41
E80Q	surface, interacts with NuoK	normal	100%,	normal	40
E80A		normal	~90%	reduced	40
Y109F	surface	NA	96%	NA	41

Supplementary Table 7. Mutations in mitochondrially encoded complex I genes (subunits ND2-ND6) associated with human diseases. The most common disease associated mutations are in bold. Abbreviations: LHON - Leber Hereditary Optic Neuropathy; MELAS - Mitochondrial Encephalopathy, Lactic Acidosis and Stroke-like episodes; HB – hydrogen bond.

Subunit Human (*E. coli*)	Human mutation: Amino acid (Nucleotide)	*E. coli* residue	*E. coli* structural location	Human disease	Effect on complex I: H – human, E – *E. coli*	Refe-rence
ND3 (NuoA)	Ser45Pro (T10191C)	Gly58	TM1-2 loop, not in structure, interface with NuoD	multiple neuro-degenerative symptoms	H: reduced activity	78, 79
	Ser34Pro (T10158C)	Asn47		mitochondrial encephalopathy	H: reduced activity	79
ND6 (NuoJ)	Ile26Met (T14596A)	Val26	surface, possibly near Q-site	LHON	H: severe cxI deficiency	80
	Gly36Ser (C14568T)	Leu36	near channel 4	LHON, secondary mutation	NA	81
	Tyr59Cys (C14498T)	Tyr59	TM3, channel 4, interface with NuoK	LHON	E: 57-93% activity	40, 81, 41
	Leu60Ser (A14495G)	Ala60	TM3, near channel 4	LHON	NA	82
	Met64Val (T14484C)	Met64	TM3, near channel 4	LHON	H: increased inhibitor sensitivity E: 78-89% activity	40, 83
	Met64Ile (C14482A) (C14482G)				E: 100% activity	40, 84
	Ala72Val (G14459A)	Met72	TM3, interface to NuoA/H	LHON / Leigh disease / dystonia	H: cxI deficiency	85
	Ala74Val **(G14453A)**	Leu74	TM3, near surface	MELAS	H: reduced activity	86
	Pro25Leu (G14600A)	Pro25	N-terminus of TM2	LHON / MELAS	H: cxI deficiency	87

Supplementary Table 7, continuation.

Subunit Human (*E. coli*)	Human mutation: Amino acid (Nucleotide)	*E. coli* residue	*E. coli* structural location	Human disease	Effect on complex I: H – human, E – *E. coli*	Refe-rence
ND5 (NuoL)	Phe124Leu (T12706C)	Phe123	near channel 1	Leigh disease	H: cxI deficiency	88
	Glu145Gly (A12770G)	Glu144	channel 1/ interface with NuoM	MELAS	NA	89
	Met237Leu (A13045C)	Met243	TM7b, interior	MELAS / LHON / Leigh disease	NA	89
	Ala458Thr (A13708G)	Ile462	lipid-facing surface	LHON	NA	90
	Asn505His (A13849C)	Trp512	TM15-TM13 HB	MELAS, secondary	NA	91
	Asp393Asn (G13513A)	Asp400	channel 2 / surface	Leigh disease	H: normal activity E: 90% activity, 70% pumping	92, 93, 94, 27
	Val243Ile (G13063A)	Val249	TM8, interior	mitochondrial disorder	H: normal assembly, reduced activity	87
	Ala236Thr (G13042A)	Ala242	TM7b, interior	LHON	NA	95
	Ala171Val (A12848T)	Ala170	near channel 1	LHON	NA	96
	Ser250Cys (A13084T)	Ala256	TM8, interior	MELAS / Leigh disease	H: cxI deficiency	97
ND4 (NuoM)	**Arg340His (G11778A)**	Arg369	surface, HB to TM7b	LHON	H: resistance to rotenone E: 63% activity, rotenone and UQ-binding affected	76, 98, 99
ND2 (NuoN)	Gly259Ser (A5244G)	Gly391	near channel 2	LHON, secondary	E: 90% activity	90, 28
	Asn150Asp (A4917G)	Ile269	near $_{L}$TM16	LHON	NA	100

Supplementary Table 8. Mutations in subunits A, D and C of Mrp antiporters.

Organism	Sub-unit	Mutation	*E. coli* residue	Expressed	Growth in high NaCl	Antiport activity	Refe-rence
Bacillus subtilis	MrpD	D75A	$_{M}$D84	+	+/-	<25%	101
		D75E		+	+	87%	101
		D75N		+	+	97%	101
		D128A	$_{M}$D135	+	-/+	10%	101
		D128E		+	+	81%	101
		D128N		+	+	100%	101
		E137A	$_{M}$E144	+	-	7%	101,102
		E137D		+	+	48%	101
		E137Q		+	-	0%	101
	MrpA	D50E	$_{L}$D82	+	+/-	40%	101, 102
		D50A		+	+	0-60%	102
		D50N		+	+	56%	101, 102
		D103A	$_{L}$D134	+	+/-	20-60%	102
		D103E		+	-/+	64%	101, 102
		D103N		+	+	76%	101, 102
		E113A	$_{L}$E144	+	-	0-30%	102
		E113D		+	-/+	60%	101, 102
		E113Q		+	-	20%	101, 102
		E657A	$_{L}$N537	+	-	<20%	102
		E657D		+	+	100%	101, 102
		E657Q		+	-/+	48%	101, 102
		D743A	Outside align-ment	+	-	NA	101, 102
		D743E		+	+	120%	101, 102
		D743N		+	-	16%	101, 102
		E747A	Outside align-ment	+	-	NA	101, 102
		E747D		+	-/+	36%	101, 102
		E747Q		+	-	4%	101, 102
Bacillus pseudo-firmus	MrpA	E140A	$_{L}$E144	+	-	10%	26
		K223A	$_{L}$K229	+	-	3%	26
		K299A	$_{L}$K305	+	-	10%	26
		G392R	$_{L}$G382	+	-	8%	26
		H230K	$_{L}$Q236	+	+/-	72%, hNaK_m*	26
		H700A	$_{L}$V550	+	+	20%, hNaK_m*	26
		H700K		+	+	64%, hNaK_m*	26
		H700W		+	+	70%, hNaK_m*	26
		Y136A	$_{L}$Y140	+	+	100%	26

* hNaK_m - high K_m for Na^+

Supplementary Table 8, continuation

Organism	Sub-unit	Mutation	*E. coli* residue	Expressed	Growth in high NaCl	Antiport activity	Refe-rence
Bacillus pseudo-firmus	MrpA	H230A	$_{L}$Q236	+	+	100%	26
		W232A	$_{L}$W238	+	+	100%	26
		Y258A	$_{L}$Y264	+	+	100%	26
		H345A	$_{L}$H334	+	+	100%	26
		G392A	$_{L}$G382	+	+	100%	26
		F405A	$_{L}$F396	+	+	100%	26
	MrpD	F135A	$_{M}$F142	+	+	100%	26
		F136T	$_{M}$W143	+	+	80%	26
		F136G		+	+/-	40%, hNaK_m*	26
		F136A		+	+	80%	26
		F136E		+	+	80%	26
		E137A	$_{M}$E144	+	-	2%	26
		E137Q		No growth	NA	NA	26
		E137D		+	+/-	100%, hNaK_m*	26
		K219A	$_{M}$K234	+	-	2%	26
		W228A	$_{M}$W243	+	+	90%	26
	MrpC	Q70A	$_{K}$Y62	+	+	80%	26
		G82I	$_{K}$S74	+	+	50%	26
		T75A	$_{K}$S67	+	-/+	100%	26
		G82P	$_{K}$S74	+	+	90%	26

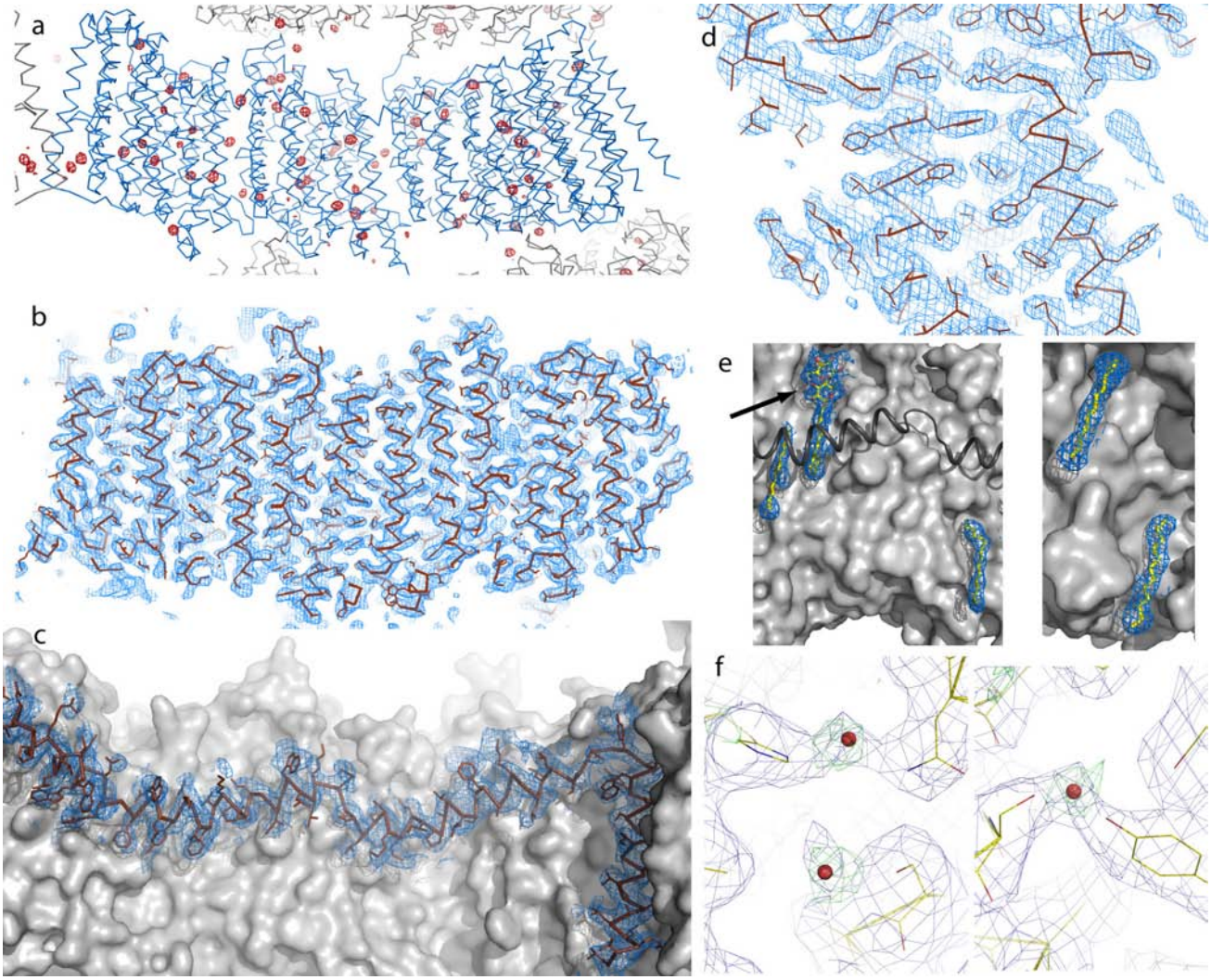

Supplementary Figure 1. Electron density of *E. coli* complex I membrane domain. **a**, Anomalous difference density map calculated using structure factors (from 20 to 3.5 Å resolution) collected at Se peak wavelength and weighted phases from the final model, shown at the level of 4 σ. **b**, Experimental map after multi-crystal (four datasets) density averaging and modification, contoured at 1 σ and overlaid on the final model. **c**, The same map displayed around the model of helix HL and surface representation of the rest of the model. **d**, Example of 2Fo-Fc map, contoured at 1.5 σ. **e**, Examples of 2Fo-Fc density corresponding to aliphatic lipid chains and a cymal-7 detergent molecule (indicated by an arrow), shown at 0.8 σ over the surface of protein. Helix HL is shown in cartoon representation. **f**, Examples of 2Fo-Fc (blue, contoured at 0.9 σ) and Fo-Fc (green, contoured at 2.7 σ) omit density around water molecules (red spheres). For density calculations, the structure was refined and density calculated without water molecules.

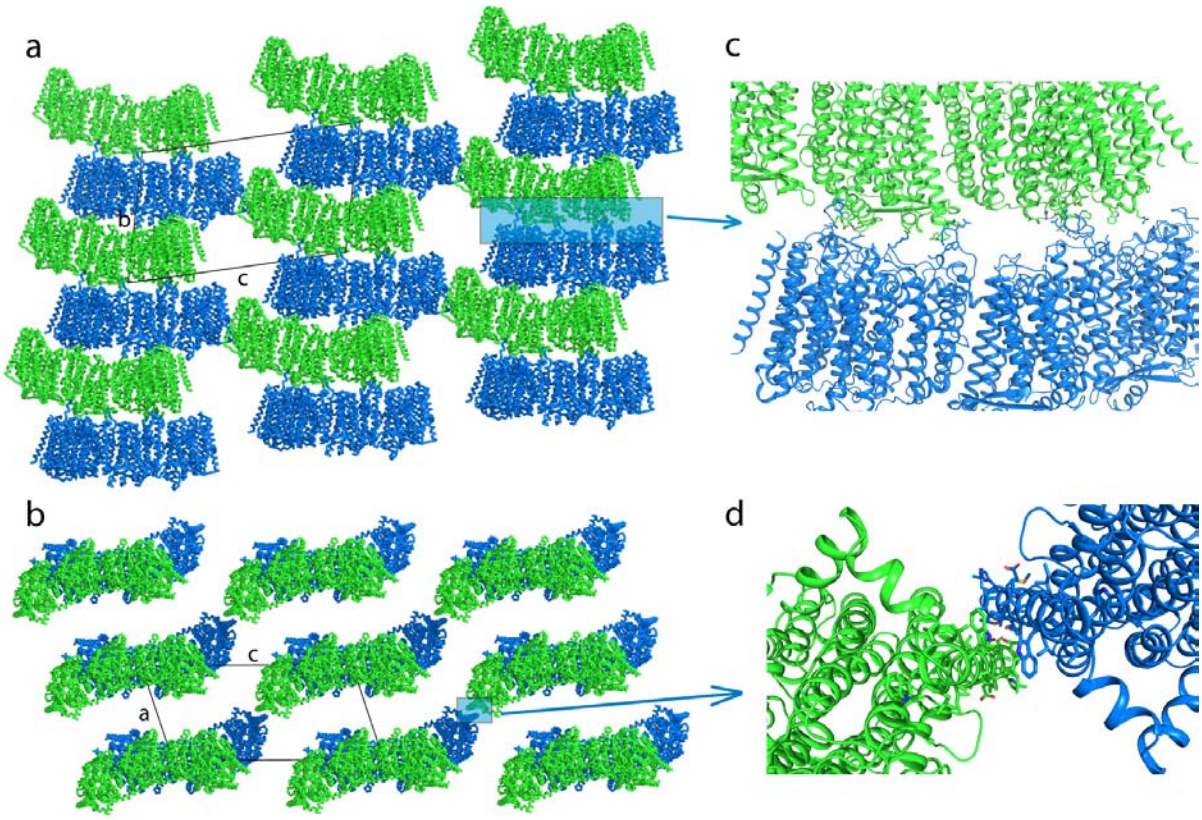

Supplementary Figure 2. Crystal packing of E. coli complex I membrane domain in space group P1. Projections along crystallographic axes *a* (**a**) and *b* (**b**). Close view of crystallographic contacts between solvent exposed loops (**c**) and membrane embedded TM16 of NuoL (**d**). No protein-protein contacts are observed along axis *a*.

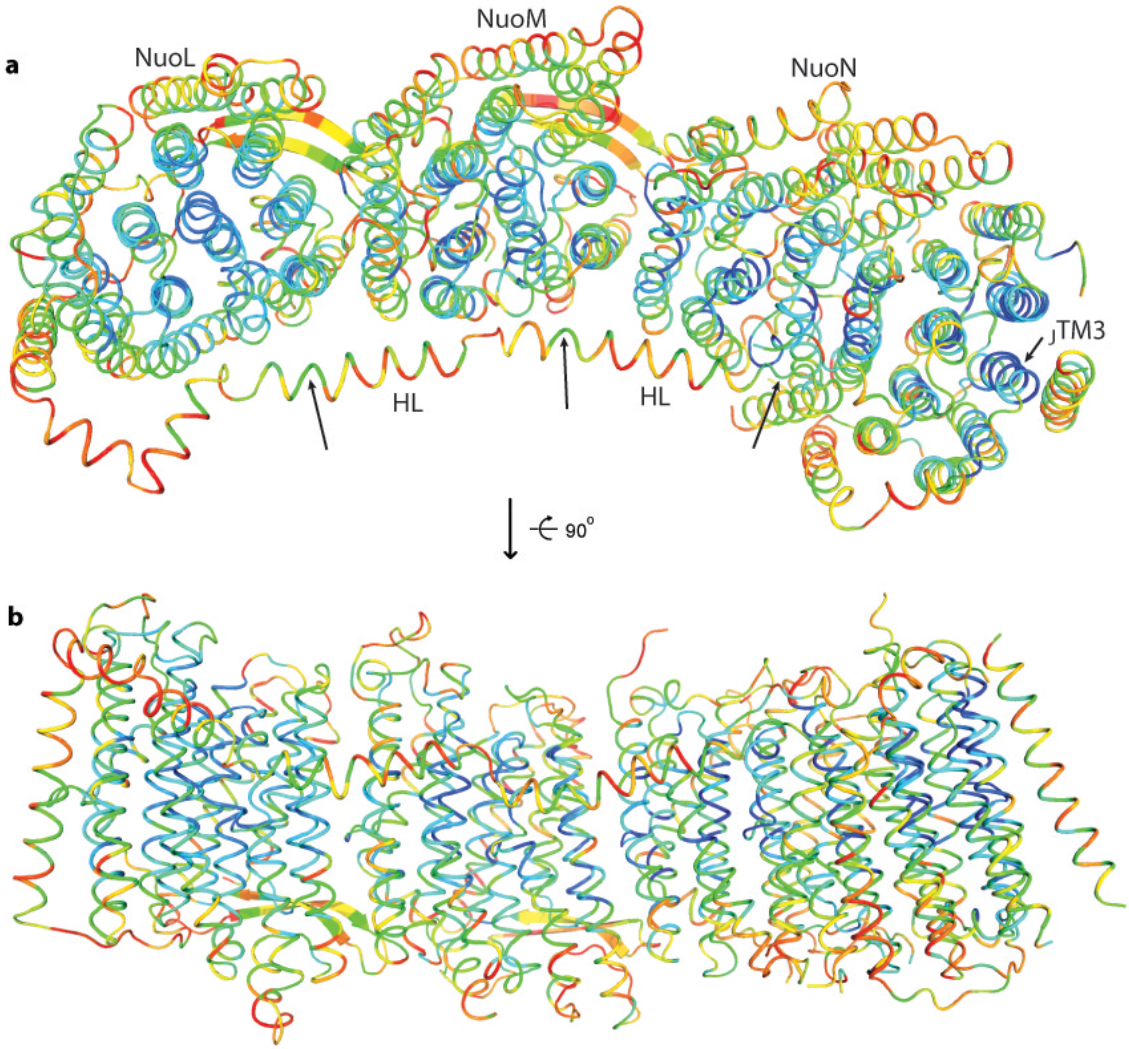

Supplementary Figure 3. Conservation of amino acid residues within the membrane domain of complex I (subunits NuoLMNAJK). Conservation degree decreases from blue (most conserved) to red (least conserved). **a**, View from the cytoplasm into membrane. Points of contact between helix HL and the main body of the domain are indicated by arrows. Highly conserved TM3 of NuoJ is indicated. **b**, Side view, similar to main text Figure 1a. The conservation degree was calculated using ConSurf server[103] and structure-based alignments of 30 sequences of complex I subunits from organisms representative of all kingdoms of life (Supplementary Fig. 7).

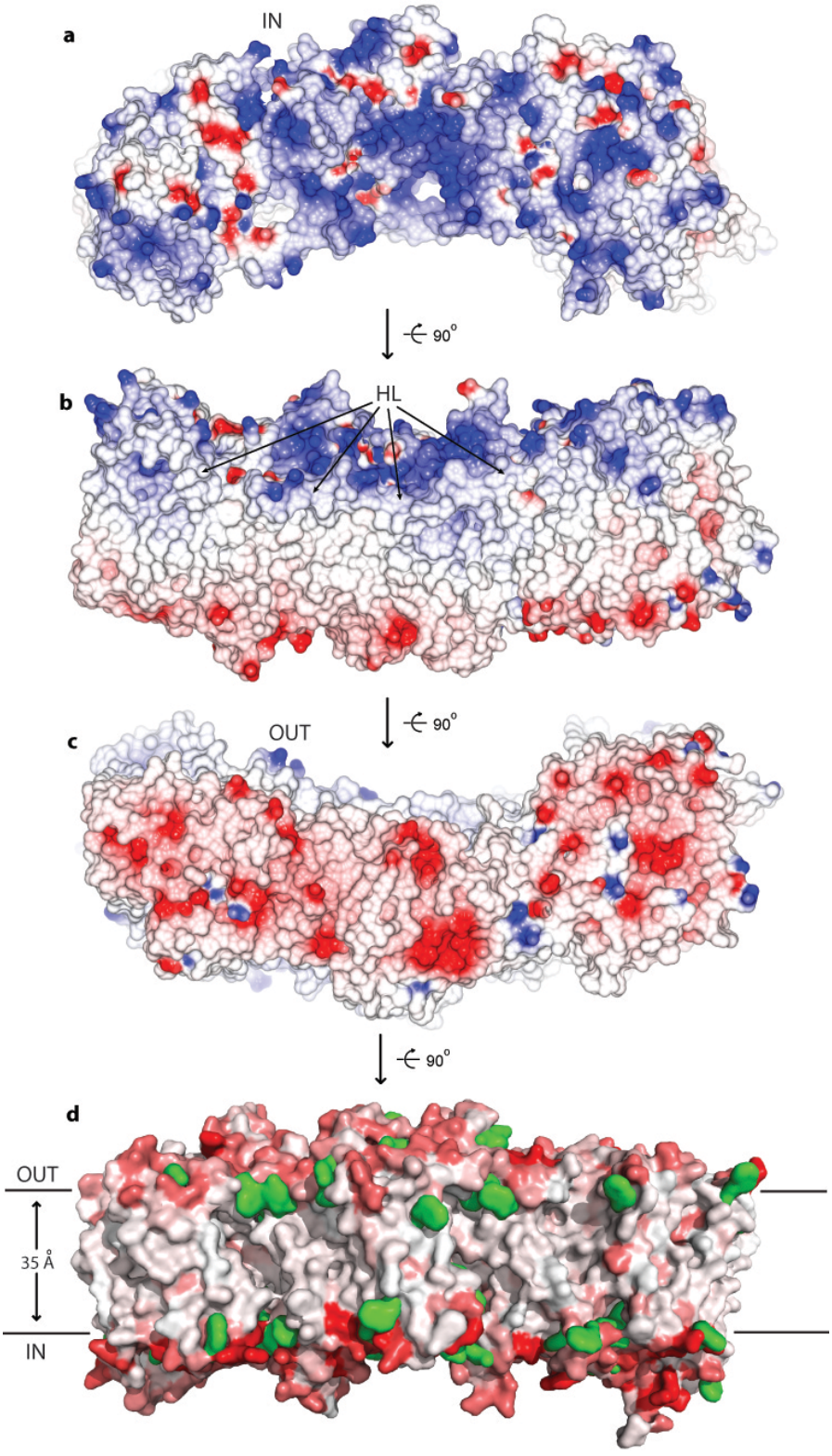

Supplementary Figure 4. Surface charge distribution of E. coli complex I membrane domain. **a**, View from the cytosol, **b**, Side view, cytosolic side up, **c**, View from the periplasm. Protein surface is shown coloured red for negative, white for neutral and blue for positive surface charges. **d**, Side view, periplasmic side up, with surface residues coloured according to the Eisenberg hydrophobicity scale[104] from white (hydrophobic) to red (hydrophilic). Surface-exposed Tyr and Trp residues are shown in green. The expected position of the lipid bilayer is indicated by black lines.

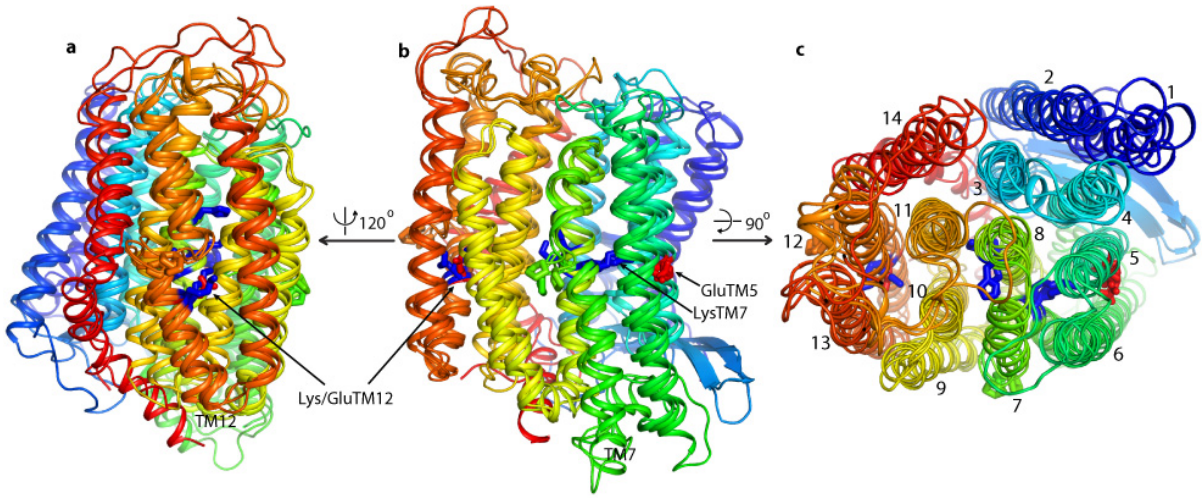

Supplementary Figure 5. Overlay of the 14 conserved helices of three antiporter-like subunits. **a,** Side view, cytoplasmic side up, centred on TM12. **b**, Side view centred on TM7. **c**, View from the cytoplasm into the membrane, with TM helices numbered. Coloured blue to red from N to C terminus. Essential charged residues are shown as sticks (GluTM5 and LysTM7 from channel one, GluTM12 from channel two and connecting $_{M}Lys^{265}$ from TM8). Conserved prolines from intra-helical loops are also shown.

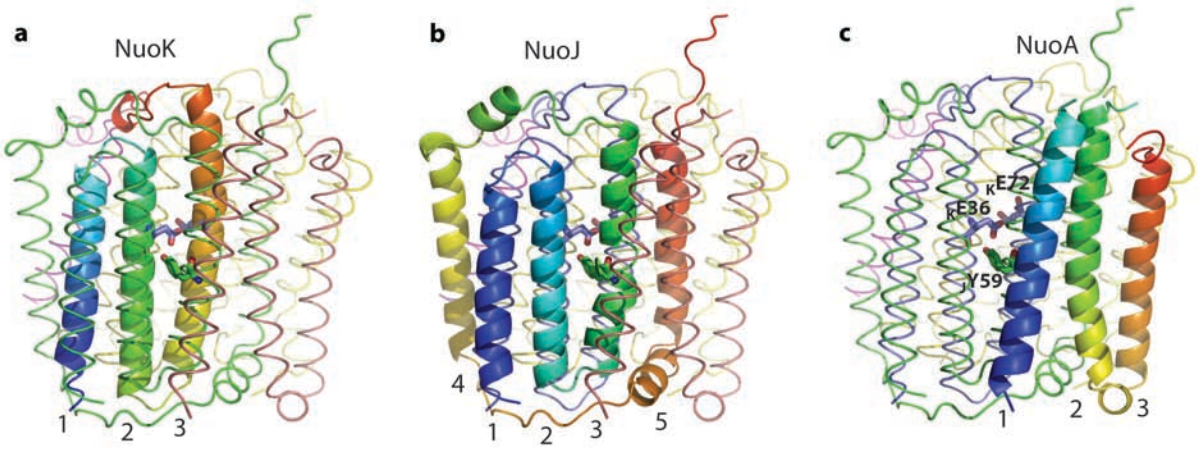

Supplementary Figure 6. Fold of subunits NuoK (a), NuoJ (b) and NuoA (c). Each subunit is highlighted in cartoon representation, coloured blue to red from N to C terminus, with TM helices numbered. Other subunits are shown as ribbons of the same colour as in Fig. 1. View in the membrane plane, cytoplasmic side up, from the interface with the hydrophilic domain. Conserved essential residues are shown as sticks ($_{K}Glu^{36}$, $_{K}Glu^{72}$ and $_{J}Tyr^{59}$).

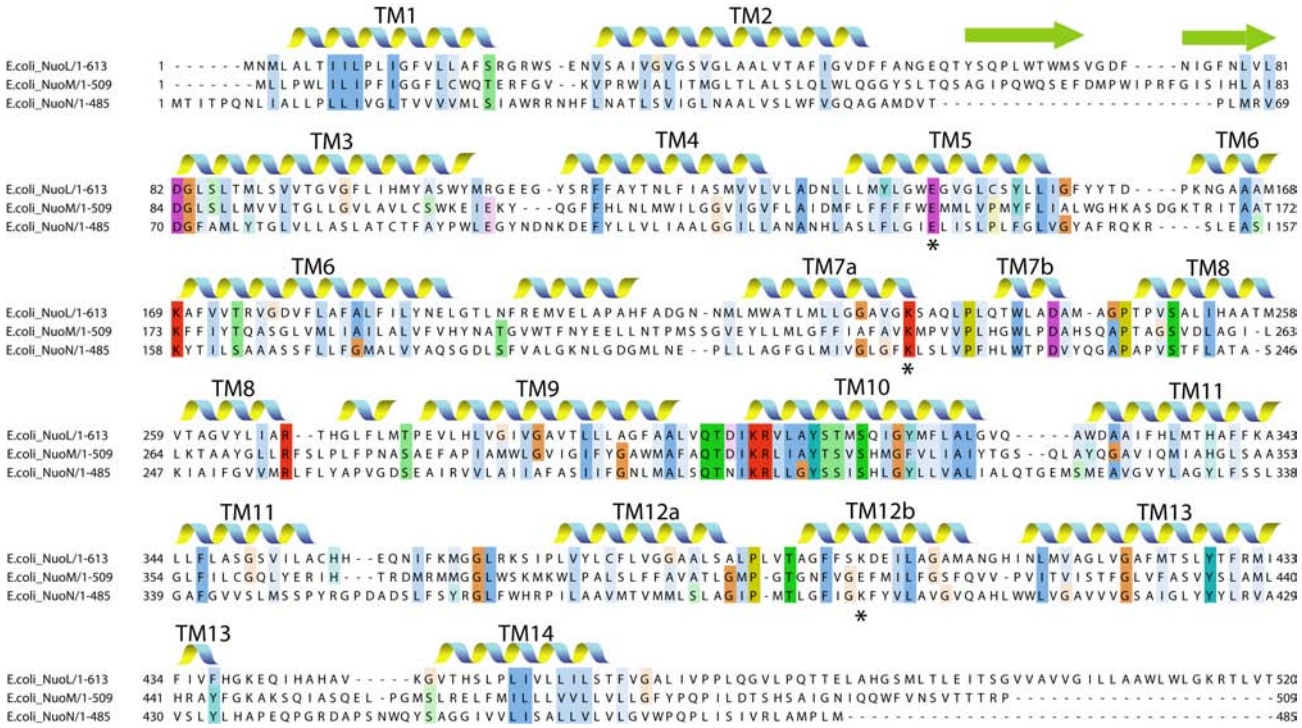

Supplementary Figure 7. Structure-based alignment of *E. coli* complex I subunits NuoL, M and N. The C-terminus of NuoL is omitted. Helices and β-strands are indicated, with TM helices labelled. The residues are coloured by conservation in Jalview[105], using Clustalx colour scheme. GluTM5, LysTM7 and Lys/GluTM12 are indicated by the asterisks.

Supplementary Figure 8. Structure-based alignment of complex I subunits NuoL/M/N/A/J/K, using 30 representatives from all kingdoms of life. Helices and β-strands are indicated, with TM helices labelled. The residues are coloured by conservation in Jalview[105], using Clustalx colour scheme. In subunits NuoL/M/N, GluTM5, LysTM7 and Lys/GluTM12 are indicated by the asterisks. Note that sequences in worms (three last sequences in the alignment) show many deviations, e.g. lacking conserved $_{N}$Glu[133], $_{K}$Glu[72] and $_{J}$Tyr[59].

a) Subunit NuoK.

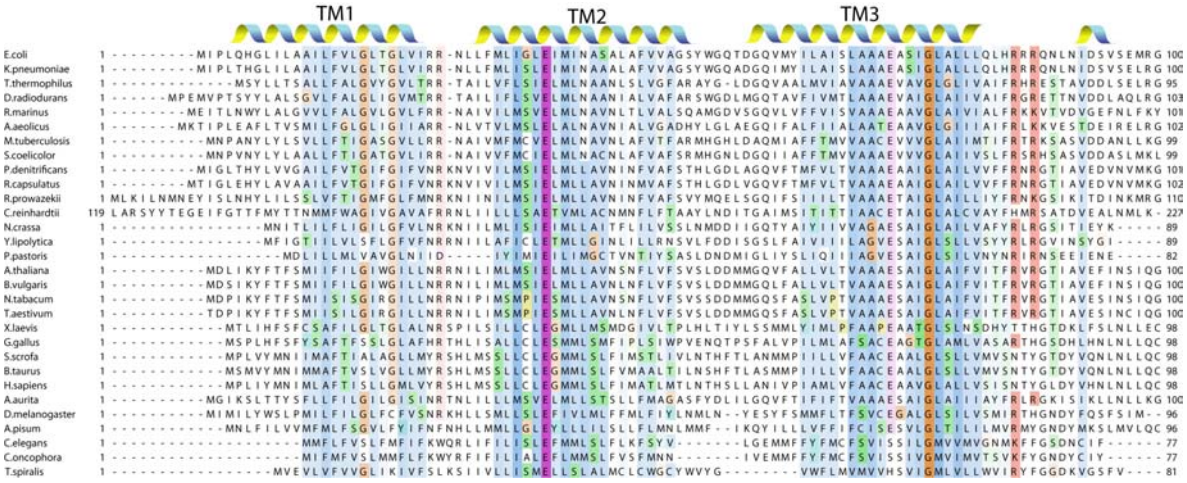

b) Subunit NuoA.

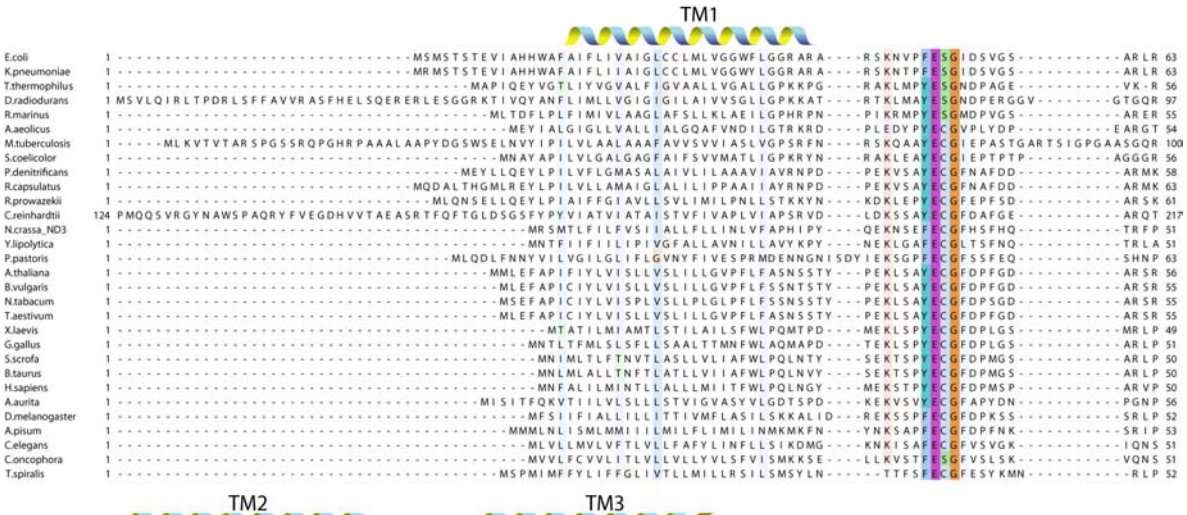

c) Subunit NuoJ.

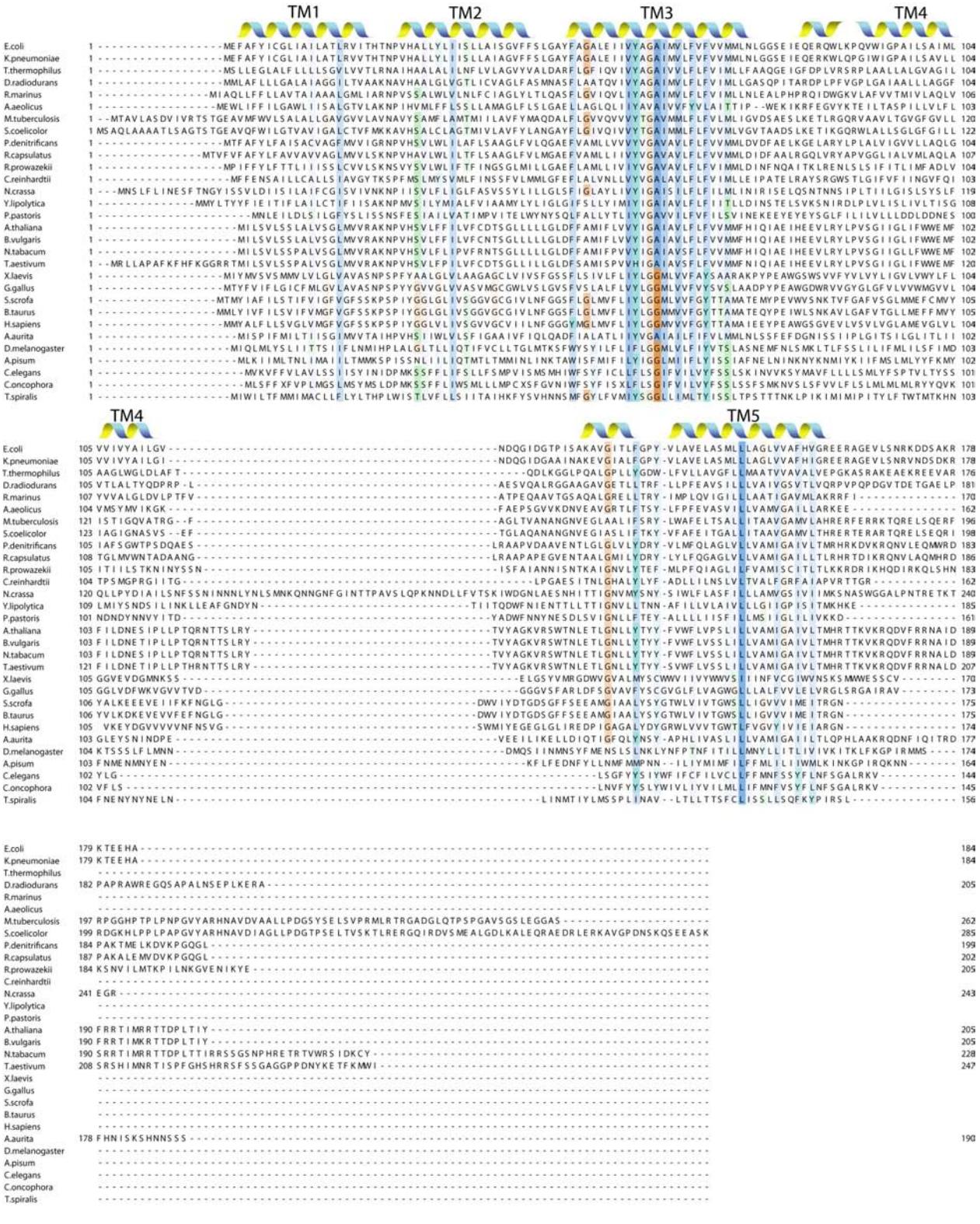

d) Subunit NuoN, part 1.

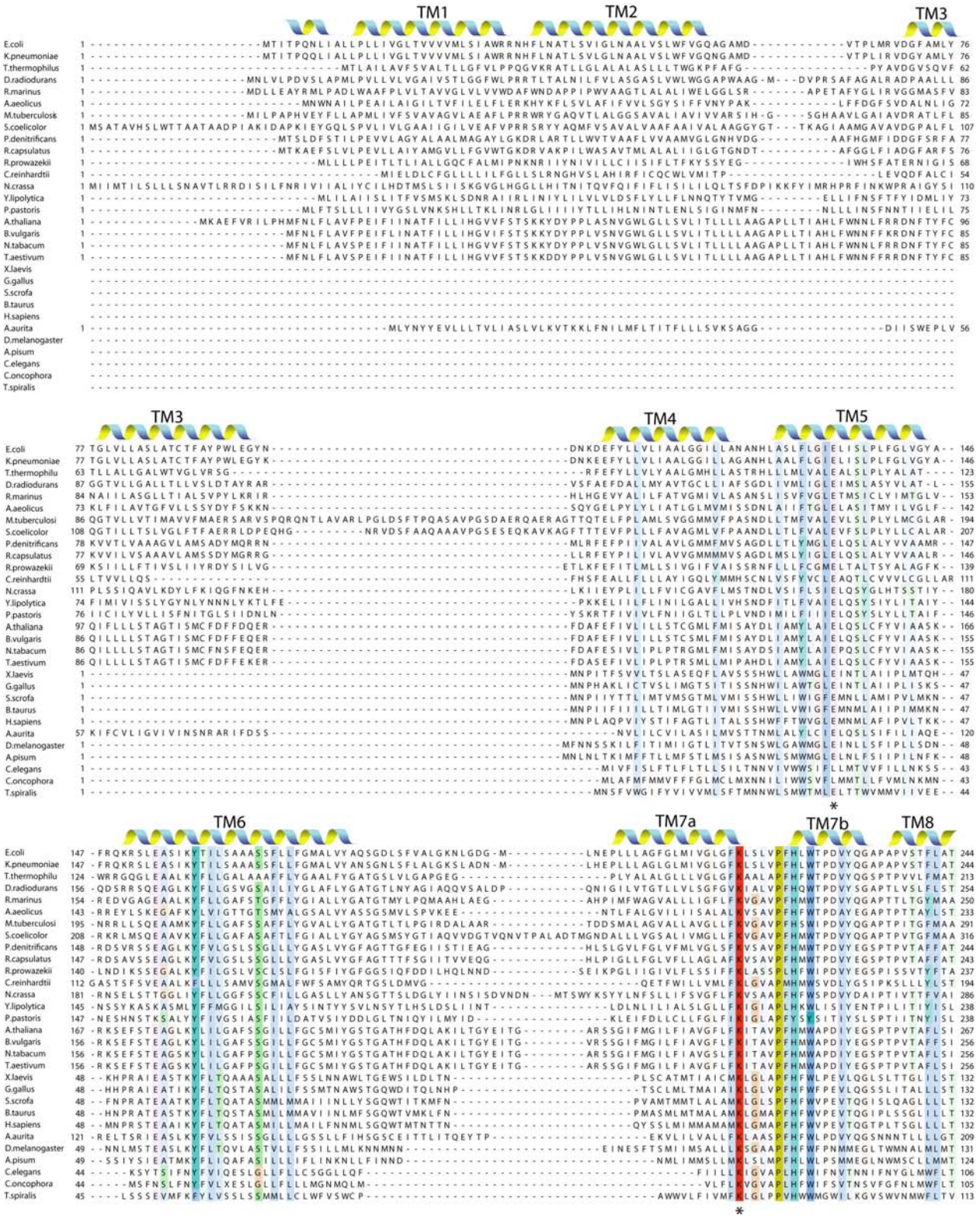

d) Subunit NuoN, part 2.

e) Subunit NuoM, part 1.

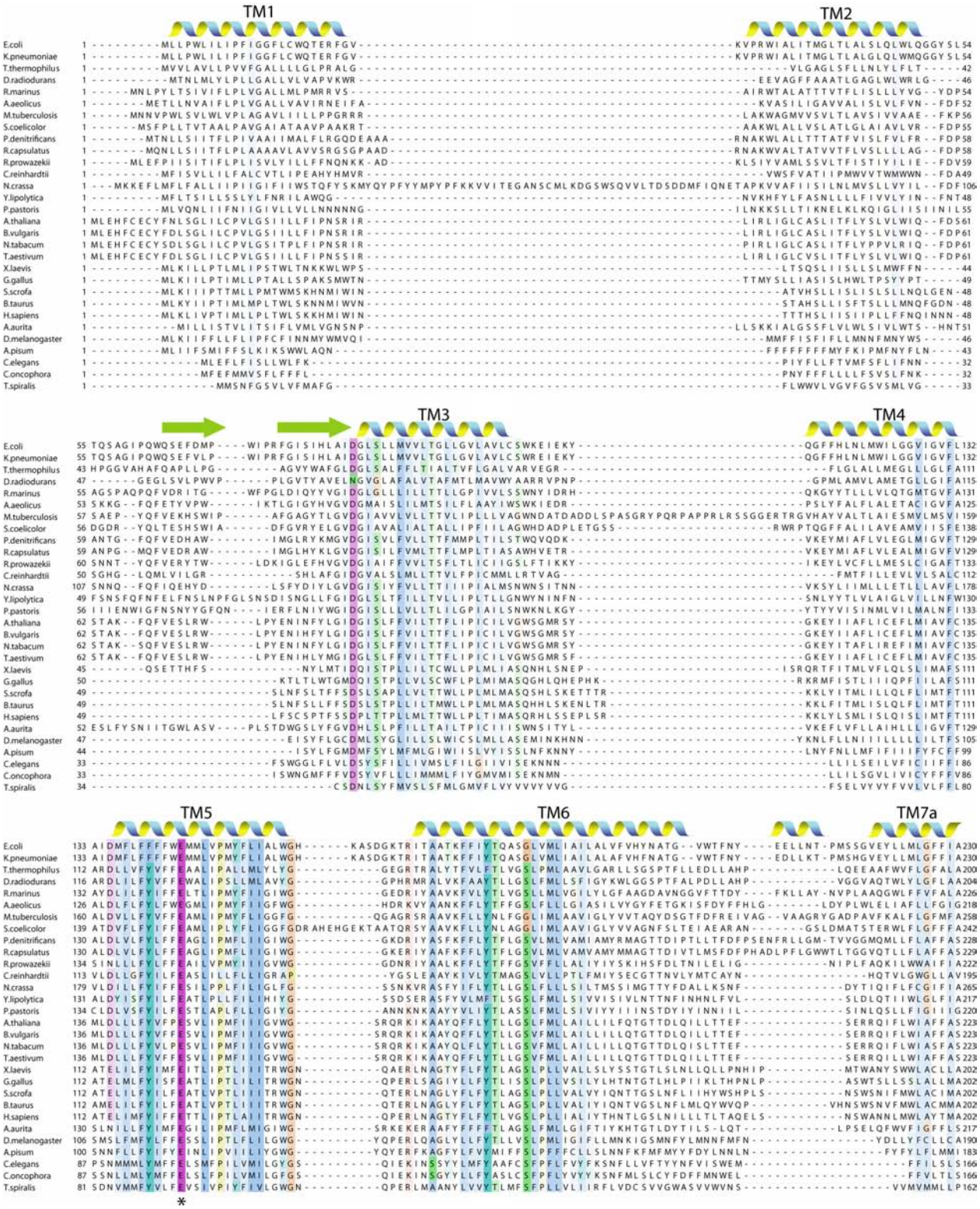

e) Subunit NuoM, part 2.

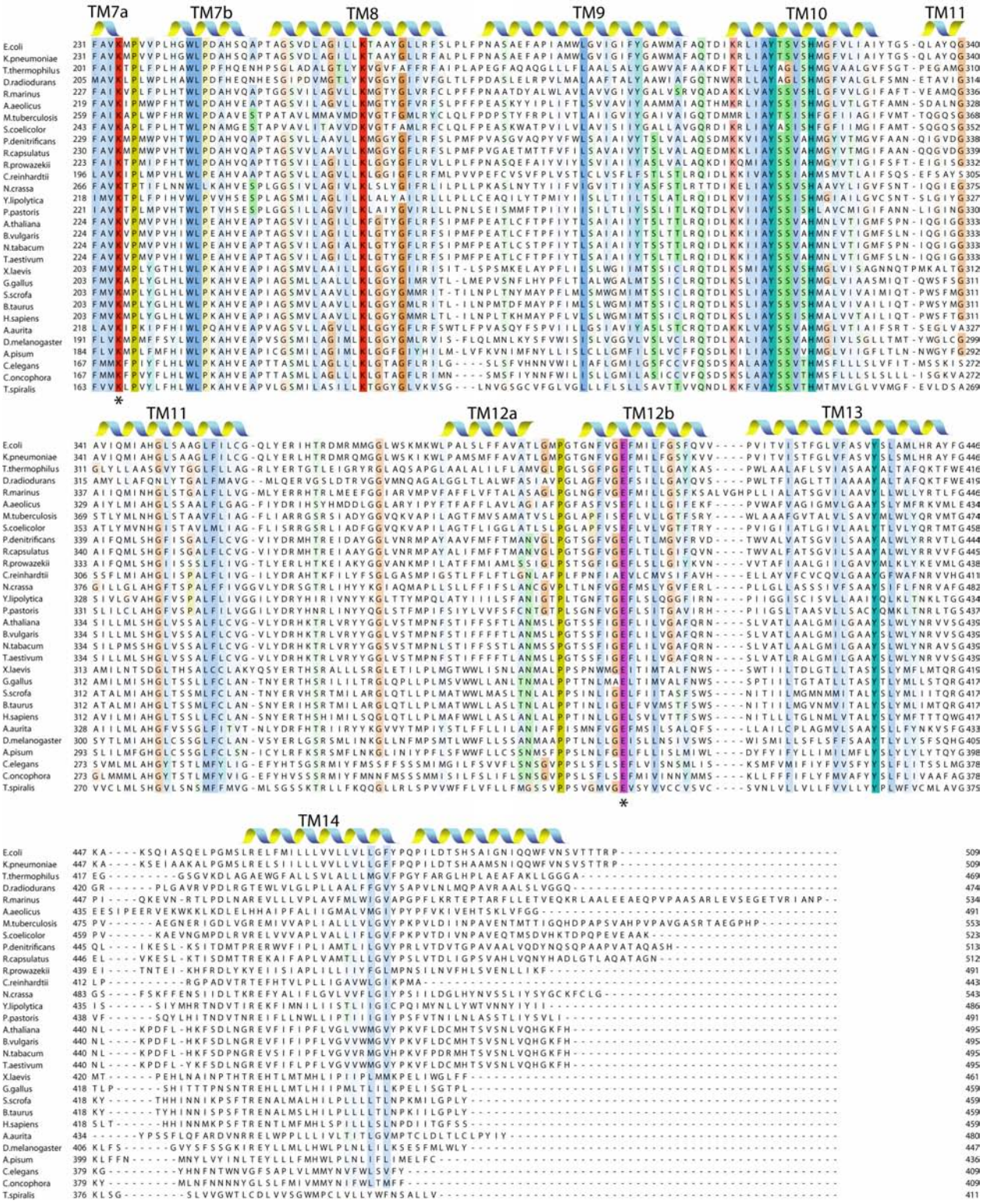

f) Subunit NuoL, part 1.

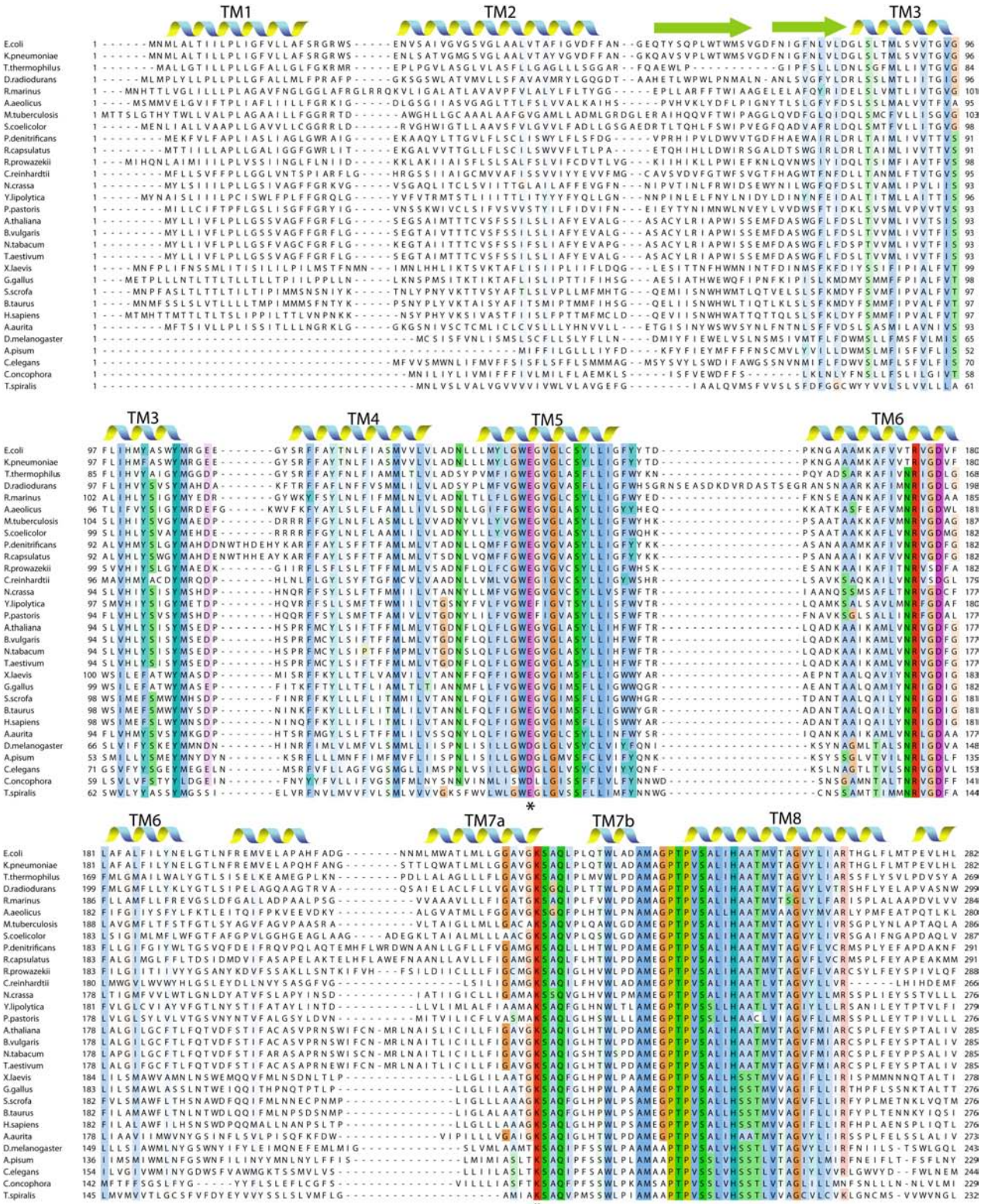

f) Subunit NuoL, part 2.

f) Subunit NuoL, part 3.

Supplementary References

61 Petrek, M. *et al.* CAVER: a new tool to explore routes from protein clefts, pockets and cavities. *BMC Bioinformatics* **7**, 316 (2006).

62 Smart, O. S., Goodfellow, J. M. & Wallace, B. A. The pore dimensions of gramicidin A. *Biophys. J.* **65**, 2455-2460 (1993).

63 Kleywegt, G. J. & Jones, T. A. Detection, delineation, measurement and display of cavities in macromolecular structures. *Acta Crystallogr. D Biol. Crystallogr.* **50**, 178-185 (1994).

64 Belevich, I. *et al.* Initiation of the proton pump of cytochrome c oxidase. *Proc. Natl. Acad. Sci. U S A* **107**, 18469-18474 (2010).

65 Buch-Pedersen, M. J., Pedersen, B. P., Veierskov, B., Nissen, P. & Palmgren, M. G. Protons and how they are transported by proton pumps. *Pflugers Arch.* **457**, 573-579 (2009).

66 Batista, A. P. & Pereira, M. M. Sodium influence on energy transduction by complexes I from Escherichia coli and Paracoccus denitrificans. *Biochim. Biophys. Acta* (2010).

67 Berrisford, J. M., Thompson, C. J. & Sazanov, L. A. Chemical and NADH-induced, ROS-dependent, cross-linking between subunits of complex I from *Escherichia coli* and *Thermus thermophilus*. *Biochemistry* **47**, 10262-10270 (2008).

68 Shaffer, P. L., Goehring, A., Shankaranarayanan, A. & Gouaux, E. Structure and mechanism of a Na+-independent amino acid transporter. *Science* **325**, 1010-1014 (2009).

69 Torres-Bacete, J., Sinha, P. K., Castro-Guerrero, N., Matsuno-Yagi, A. & Yagi, T. Features of subunit NuoM (ND4) in Escherichia coli NDH-1: topology and implication of conserved Glu144 for coupling site 1. *J. Biol. Chem.* **284**, 33062-33069 (2009).

70 Nakamaru-Ogiso, E. *et al.* The ND2 subunit is labeled by a photoaffinity analogue of asimicin, a potent complex I inhibitor. *FEBS Lett.* **584**, 883-888 (2010).

71 Gong, X. *et al.* The ubiquinone-binding site in NADH:ubiquinone oxidoreductase from *Escherichia coli*. *J. Biol. Chem.* **278**, 25731-25737 (2003).

72 Shinzawa-Itoh, K. *et al.* Bovine heart NADH-ubiquinone oxidoreductase contains one molecule of ubiquinone with ten isoprene units as one of the cofactors. *Biochemistry* **49**, 487-492 (2010).

73 Birrell, J. A. & Hirst, J. Truncation of subunit ND2 disrupts the threefold symmetry of the antiporter-like subunits in complex I from higher metazoans. *FEBS Lett.* **584**, 4247-4252 (2010).

74 Galkin, A., Drose, S. & Brandt, U. The proton pumping stoichiometry of purified mitochondrial complex I reconstituted into proteoliposomes. *Biochim. Biophys. Acta* **1757**, 1575-1581 (2006).

75 Brandt, U. A two-state stabilization-change mechanism for proton-pumping complex I. *Biochim. Biophys. Acta* (2011).

76 Torres-Bacete, J., Nakamaru-Ogiso, E., Matsuno-Yagi, A. & Yagi, T. Characterization of the NuoM (ND4) subunit in Escherichia coli NDH-1:

conserved charged residues essential for energy-coupled activities. *J. Biol. Chem.* **282**, 36914-36922 (2007).

77 Kao, M. C. *et al.* Functional roles of four conserved charged residues in the membrane domain subunit NuoA of the proton-translocating NADH-quinone oxidoreductase from Escherichia coli. *J. Biol. Chem.* **279**, 32360-32366 (2004).

78 Taylor, R. W., Singh-Kler, R., Hayes, C. M., Smith, P. E. & Turnbull, D. M. Progressive mitochondrial disease resulting from a novel missense mutation in the mitochondrial DNA ND3 gene. *Ann. Neurol.* **50**, 104-107 (2001).

79 McFarland, R. *et al.* De novo mutations in the mitochondrial ND3 gene as a cause of infantile mitochondrial encephalopathy and complex I deficiency. *Ann. Neurol.* **55**, 58-64 (2004).

80 De Vries, D. D. *et al.* Genetic and biochemical impairment of mitochondrial complex I activity in a family with Leber hereditary optic neuropathy and hereditary spastic dystonia. *Am. J. Hum. Genet.* **58**, 703-711 (1996).

81 Wissinger, B. *et al.* Mutation analysis of the ND6 gene in patients with Lebers hereditary optic neuropathy. *Biochem. Biophys. Res. Commun.* **234**, 511-515 (1997).

82 Chinnery, P. F. *et al.* The mitochondrial ND6 gene is a hot spot for mutations that cause Leber's hereditary optic neuropathy. *Brain* **124**, 209-218 (2001).

83 Carelli, V. *et al.* Biochemical features of mtDNA 14484 (ND6/M64V) point mutation associated with Leber's hereditary optic neuropathy. *Ann. Neurol.* **45**, 320-328 (1999).

84 Valentino, M. L. *et al.* Mitochondrial DNA nucleotide changes C14482G and C14482A in the ND6 gene are pathogenic for Leber's hereditary optic neuropathy. *Ann. Neurol.* **51**, 774-778 (2002).

85 Kirby, D. M., Kahler, S. G., Freckmann, M. L., Reddihough, D. & Thorburn, D. R. Leigh disease caused by the mitochondrial DNA G14459A mutation in unrelated families. *Ann. Neurol.* **48**, 102-104 (2000).

86 Ravn, K. *et al.* An mtDNA mutation, 14453G-->A, in the NADH dehydrogenase subunit 6 associated with severe MELAS syndrome. *Eur. J. Hum. Genet.* **9**, 805-809 (2001).

87 Malfatti, E. *et al.* Novel mutations of ND genes in complex I deficiency associated with mitochondrial encephalopathy. *Brain* **130**, 1894-1904 (2007).

88 Taylor, R. W., Morris, A. A., Hutchinson, M. & Turnbull, D. M. Leigh disease associated with a novel mitochondrial DNA ND5 mutation. *Eur. J. Hum. Genet.* **10**, 141-144 (2002).

89 Liolitsa, D., Rahman, S., Benton, S., Carr, L. J. & Hanna, M. G. Is the mitochondrial complex I ND5 gene a hot-spot for MELAS causing mutations? *Ann. Neurol.* **53**, 128-132 (2003).

90 Brown, M. D. *et al.* Mitochondrial DNA complex I and III mutations associated with Leber's hereditary optic neuropathy. *Genetics* **130**, 163-173 (1992).

91 Choi, B. O. *et al.* A MELAS syndrome family harboring two mutations in mitochondrial genome. *Exp. Mol. Med.* **40**, 354-360 (2008).

92 Brautbar, A. *et al.* The mitochondrial 13513G>A mutation is associated with Leigh disease phenotypes independent of complex I deficiency in muscle. *Mol. Genet. Metab.* **94**, 485-490 (2008).

93 Pulkes, T. *et al.* The mitochondrial DNA G13513A transition in ND5 is associated with a LHON/MELAS overlap syndrome and may be a frequent cause of MELAS. *Ann. Neurol.* **46**, 916-919 (1999).
94 Kirby, D. M. *et al.* Low mutant load of mitochondrial DNA G13513A mutation can cause Leigh's disease. *Ann. Neurol.* **54**, 473-478 (2003).
95 Valentino, M. L. *et al.* The 13042G --> A/ND5 mutation in mtDNA is pathogenic and can be associated also with a prevalent ocular phenotype. *J. Med. Genet.* **43**, e38 (2006).
96 Mayorov, V., Biousse, V., Newman, N. J. & Brown, M. D. The role of the ND5 gene in LHON: characterization of a new, heteroplasmic LHON mutation. *Ann. Neurol.* **58**, 807-811 (2005).
97 Crimi, M. *et al.* A missense mutation in the mitochondrial ND5 gene associated with a Leigh-MELAS overlap syndrome. *Neurology* **60**, 1857-1861 (2003).
98 Wallace, D. C. *et al.* Mitochondrial DNA mutation associated with Leber's hereditary optic neuropathy. *Science* **242**, 1427-1430 (1988).
99 Carelli, V. *et al.* Leber's hereditary optic neuropathy: biochemical effect of 11778/ND4 and 3460/ND1 mutations and correlation with the mitochondrial genotype. *Neurology* **48**, 1623-1632 (1997).
100 Johns, D. R. & Berman, J. Alternative, simultaneous complex I mitochondrial DNA mutations in Leber's hereditary optic neuropathy. *Biochem. Biophys. Res. Commun.* **174**, 1324-1330 (1991).
101 Kajiyama, Y., Otagiri, M., Sekiguchi, J., Kudo, T. & Kosono, S. The MrpA, MrpB and MrpD subunits of the Mrp antiporter complex in Bacillus subtilis contain membrane-embedded and essential acidic residues. *Microbiology* **155**, 2137-2147 (2009).
102 Kosono, S. *et al.* Functional involvement of membrane-embedded and conserved acidic residues in the ShaA subunit of the multigene-encoded Na+/H+ antiporter in Bacillus subtilis. *Biochim. Biophys. Acta* **1758**, 627-635 (2006).
103 Landau, M. *et al.* ConSurf 2005: the projection of evolutionary conservation scores of residues on protein structures. *Nucl. Acids Res.* **33**, W299-302 (2005).
104 Eisenberg, D., Schwarz, E., Komarony, M. & Wall, R. Normalized consensus hydrophobicity scale. *J. Mol. Biol.* **179**, 125-142 (1984).
105 Waterhouse, A. M., Procter, J. B., Martin, D. M. A., Clamp, M. & Barton, G. J. Jalview Version 2-a multiple sequence alignment editor and analysis workbench. *Bioinformatics* **25**, 1189-1191 (2009).